Recent Developments in the Flux Reconstruction Method and Extensions to Large Eddy Simulation

Prof. Antony Jameson

Department of Aeronautics & Astronautics
– *Aerospace Computing Laboratory* –
Stanford University
jameson@baboon.stanford.edu

SIAM Conference on Computational Science and Engineering
February 25–March 1, 2013
Boston, MA

Outline

History of CFD in Van Leer's View

Top level: Jay Boris, Vladimir Kolgan, Bram van Leer, Antony Jameson
Ground level: Richard Courant, Kurt Friedrichs, Hans Lewy, Robert MacCormack, Philip Roe, John von Neumann, Stanley Osher, Amiram Harten, Peter Lax, Sergei Godunov

Emergence of CFD

- In 1960 the underlying principles of fluid dynamics and the formulation of the governing equations (potential flow, Euler, RANS) were well established
- The new element was the emergence of powerful enough computers to make numerical solution possible – to carry this out required new algorithms
- The emergence of CFD in the 1965–2005 period depended on a combination of advances in computer power and algorithms.

Some significant developments in the '60s:

- birth of commercial jet transport – B707 & DC-8
- intense interest in transonic drag rise phenomena
- lack of analytical treatment of transonic aerodynamics
- birth of supercomputers – CDC6600

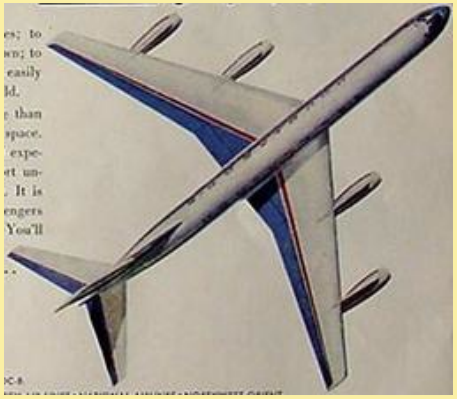

DC-8

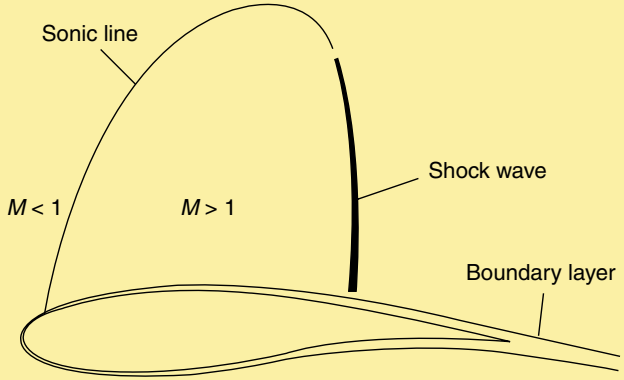

Transonic Flow

CDC6600

Multi-Disciplinary Nature of CFD

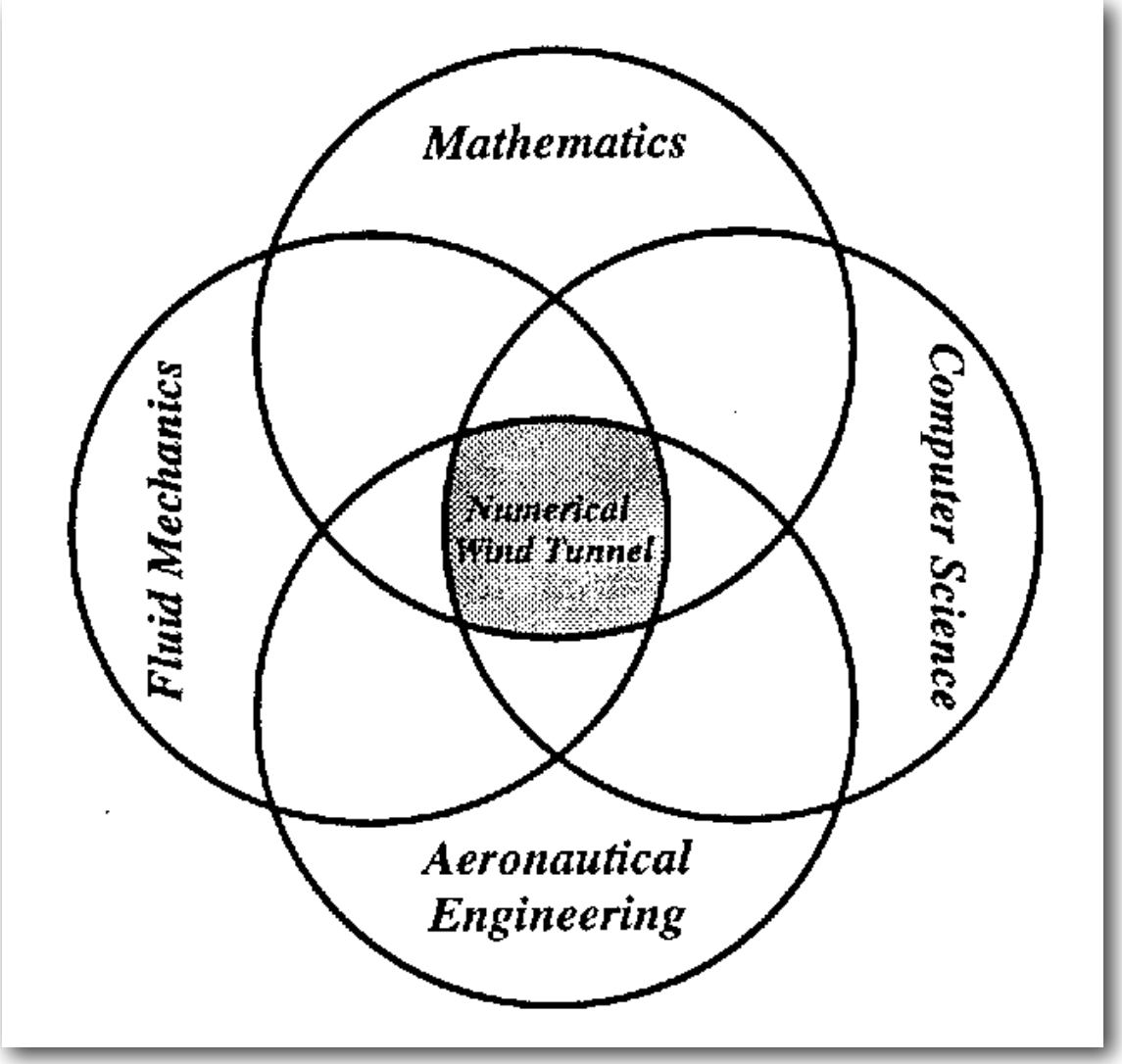

50 Years of CFD

- 1960–1970: **Early Developments**

  Riemann-based schemes for gas dynamics (Godunov), 2nd-order dissipative schemes for hyperbolic equations (Lax-Wendroff), efficient explicit methods for Navier-Stokes (MacCormack), panel method (Hess-Smith)

- 1970–1980: **Potential Flow Equations**

  type-dependent differencing (Murman-Cole), complex characteristics (Garabedian), rotated difference (Jameson), multigrids (Brandt), complete airplane solution (Glowinsky)

- 1980–1990: **Euler and Navier-Stokes Equations**

  oscillation control via limiters (Boris-Book), high-order Godunov scheme (van Leer), flux splitting (Steger-Warming), shock capturing via controlled diffusion (Jameson-Schmit-Turkel), approximate Riemann solver (Roe), total variation diminishing (Harten), multigrids (Jameson, Ni), solution of complete airplane (Jameson-Baker-Weatherill)

- 1990–2000: **Aerodynamic Shape Optimization**

  adjoint based control theory

- 2000–2010: **Discontinuous Finite Element Methods**

  Discontinuous Galerkin, Spectral Difference, Flux Reconstruction, *etc.*

Advances in Computer Power

1970	CDC6600	1 Megaflops	10^6
1980	Cray 1 Vector Computer	100 Megaflops	10^8
1994	IBM SP2 Parallel Computer	10 Gigaflops	10^{10}
2007	Linux Clusters	100 Teraflops	10^{14}
2007	(affordable) Box Cluster in my house Four 3 GHz dual core CPUs (24 Gigaflops peak) $10,000	2.5 Gigaflops	2.5×10^9
2009	HP Pavilion Quadcore Notebook $1,099	1 Gigaflops	10^9
2011	MacBook Pro Quadcore Laptop $2,099	2.5 Gigaflops	2.5×10^9

Outline

The Cost of the Degrees of Freedom

Fluid dynamic problems involve polynomials with large N and fairly large p

Complexity of Fluid Dynamic Simulations - Explicit Schemes

- With $N \approx n^3$ mesh points in 3D and explicit time stepping, each time step requires $O(n^3)$ operations
- The time step of a stable scheme is proportional to the mesh interval h divided by the wave speed, and $h \approx 1/n$, giving complexity $Cn^4 \approx N^{4/3}$ with a constant C depending on the algorithm

Complexity of Fluid Dynamic Simulations - Implicit Schemes

- An implicit scheme requires matrix inversion at each time step with complexity NB^2 where B is the bandwidth $\approx$ n^2, so the cost of a step is $O(n^7)$
- The time step is not limited by the mesh interval, so the number of time steps is independent of n, giving total complexity $\approx$ n^7

Grid Size for a Transport Aircraft Wing

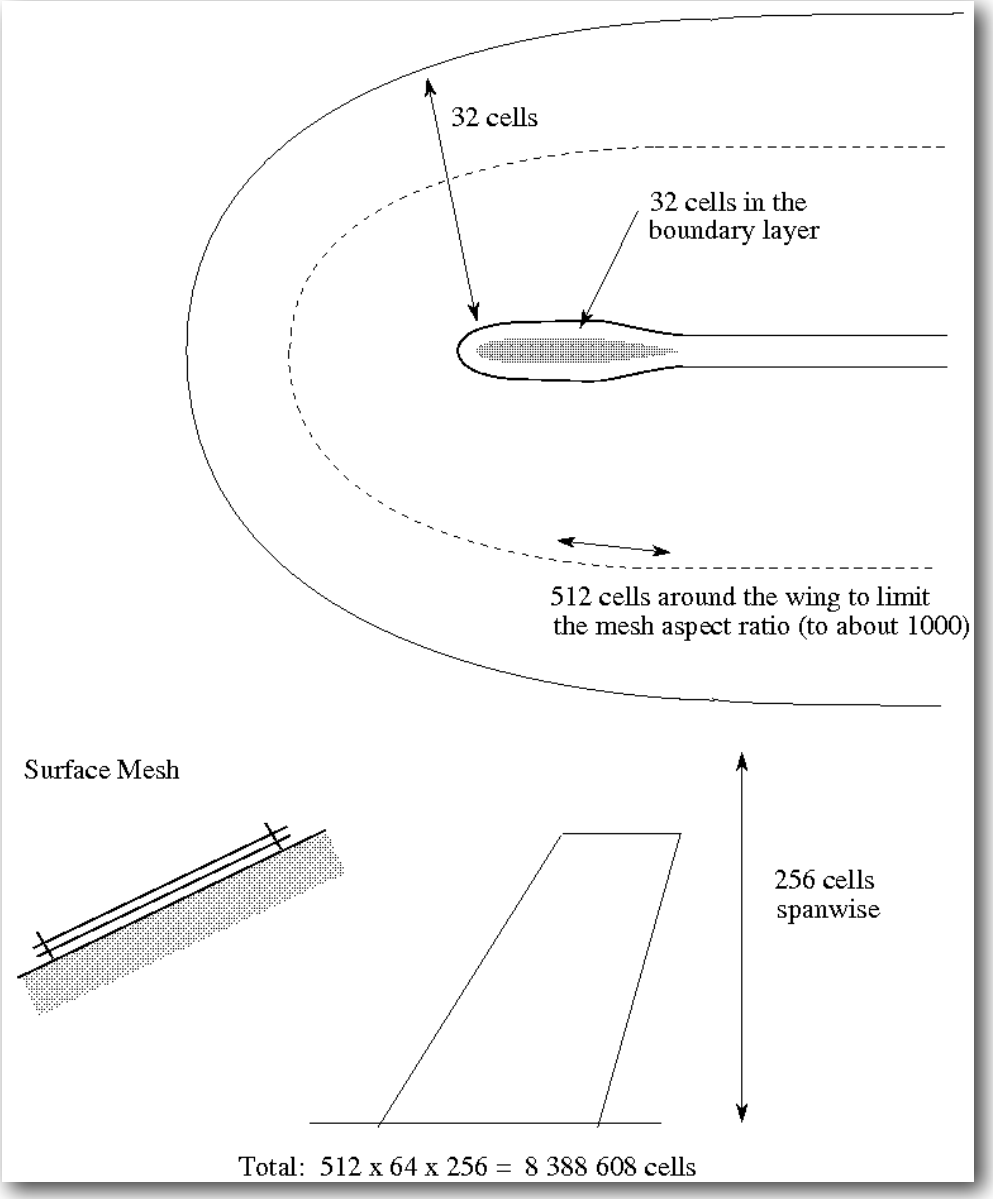

Complexity of CFD in the '70s

- The complexity of a 3D prediction of transonic flow is $O(n^4)$ and reasonable accuracy can be obtained with $n \approx 100$
- Calculations could be completed in $O(10^8)$ operations with a CDC 6600 which could achieve $\approx 10^6$ flops
- Thus a useful 3D calculation might be possible in $O(10^2)$ seconds
- The author recognized this in 1971
- Actually FLO22 (Jameson and Caughey), which was the first program which could actually predict transonic flow over a swept wing with engineering accuracy, required about 10,000 seconds for a solution

Complexity of CFD in the '80s

- 800,000 mesh cells for a viscous mesh around a wing
- 5,000 flops per solution step using FLO107
- 300 steps for the solution to converge
- $(8 \times 10^5) \times (5 \times 10^3) \times (3 \times 10^2) = 1.2 \times 10^{12}$

Roughly 10^{12} flops for RANS simulation on 0.8 million mesh cells

With a 1 Gigaflop computer, solution takes about 1,000 seconds...

... About 400 seconds with a 2011 MacBook Pro quadcore at 2.5 Gflops

CFD Complexity for Turbulent Flow Simulations

- For a turbulent flow with a Reynolds number Re, the length scale of the smallest eddies relative to the integral length scale $\approx Re^{-3/4}$ (Kolmogorov, 1943)
- With a comparable time step, the complexity of the simulations $\approx Re^3$
- For a jumbo jet such as the Airbus A380, $Re \approx 10^8$
- Direct Numerical Simulation (DNS) of the flow over the A380 has a complexity $\approx 10^{24}$ operations
- With a Petaflop computer (IBM Roadrunner, 2008), DNS of the A380 has a complexity of about 10^9 seconds

About 30 Years!

Outline

Impact of CFD on Configuration Lines & Wind Tunnel Testing

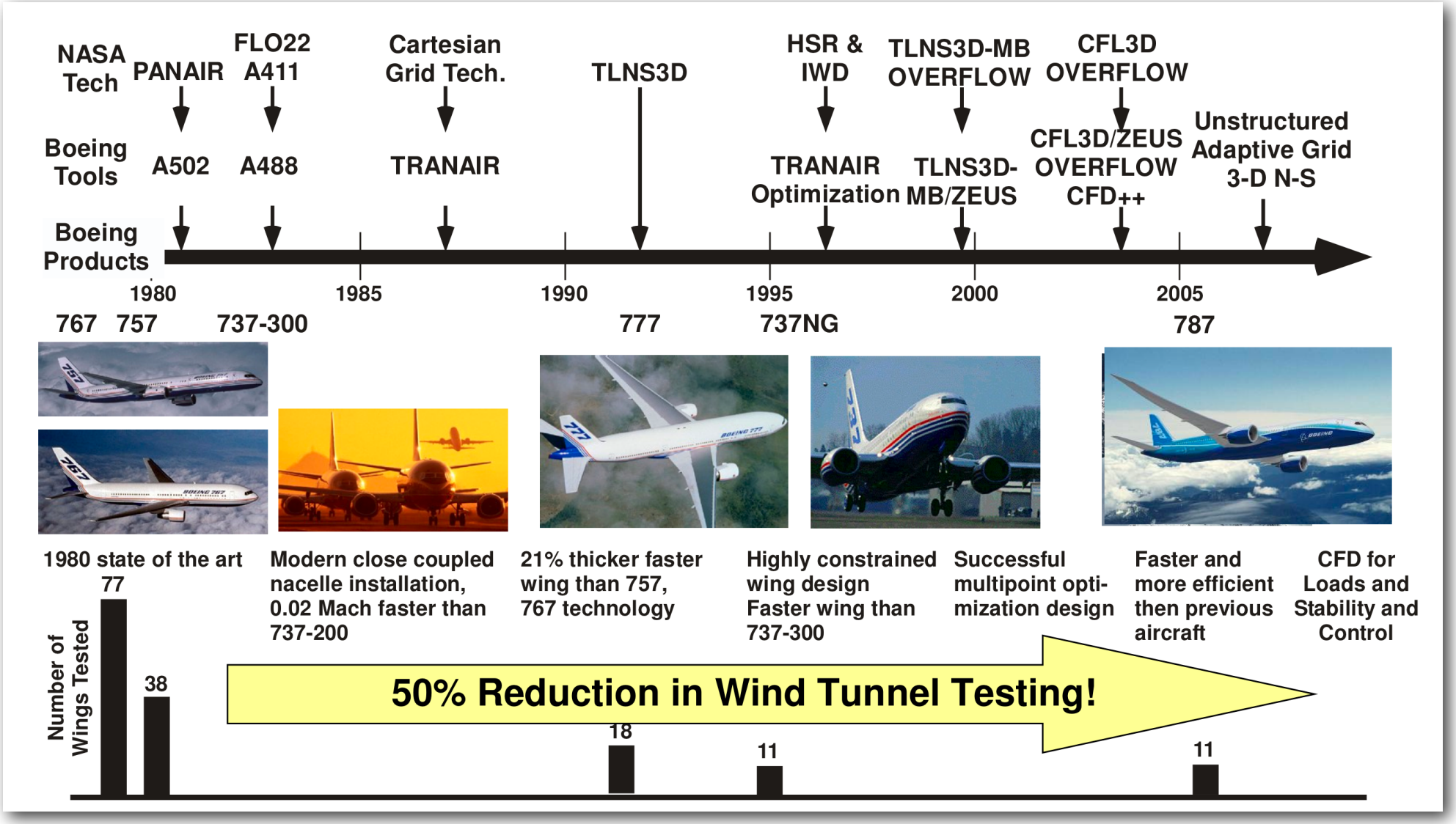

Computational Methods at Boeing

TRANAIR:

- Full Potential with directly coupled Boundary Layer
- Cartesian solution adaptive grid
- Drela lag-dissipation turbulence model
- Multi-point design/optimization

Navier-Stokes Codes:

- CFL3D – Structured Multiblock Grid
- TLNS3D – Structured Multiblock Grid, Thin Layer
- OVERFLOW – Overset Grid

N-S Turbulence Models:

- S-A Spalart-Allmaras
- Menter's k-ω SST

CFD Contributions to B787

CFD Development for Aircraft Design

MEGAFLOW / MEGADESIGN
- National CFD Initiative (since 1995)

Development & validation of a national CFD software for complete aircraft applications which

- allows computational aerodynamic analysis for 3D complex configurations at cruise, high-lift & off-design conditions
- builds the basis for shape optimization and multidisciplinary simulation
- establishes numerical flow simulation as a routinely used tool at DLR and in German aircraft industry
- serves as a development platform for universities

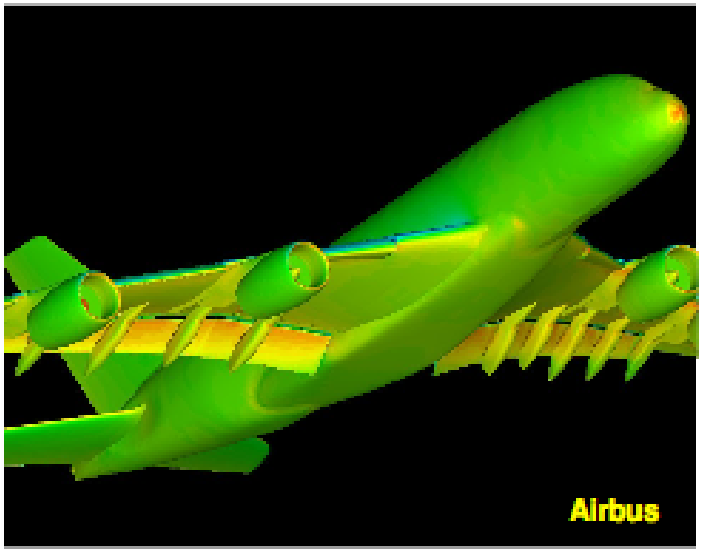

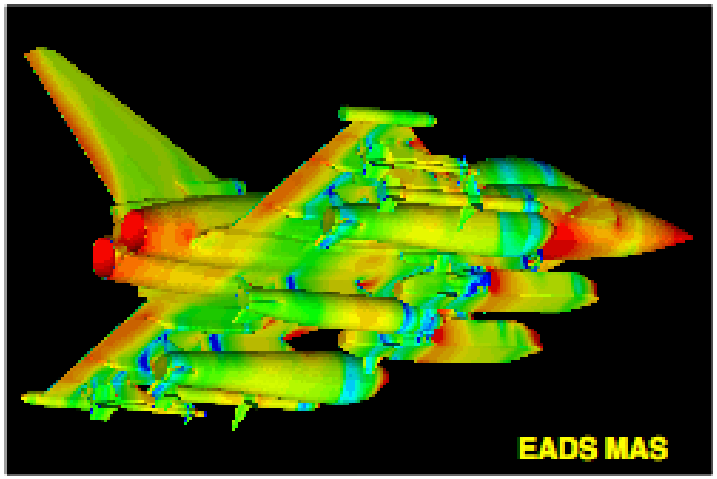

Unstructured RANS Capability: TAU

Tool for complex configurations

- hybrid meshes, cell vertex / cell centered
- high-level turbulence & transition models (RSM, DES, linear stability methods)
- state-of-the-art algorithms (JST, multigrid, ...)
- local mesh adaptation
- chimera technique
- fluid / structure coupling
- continuous/discrete adjoint
- extensions to hypersonic flows

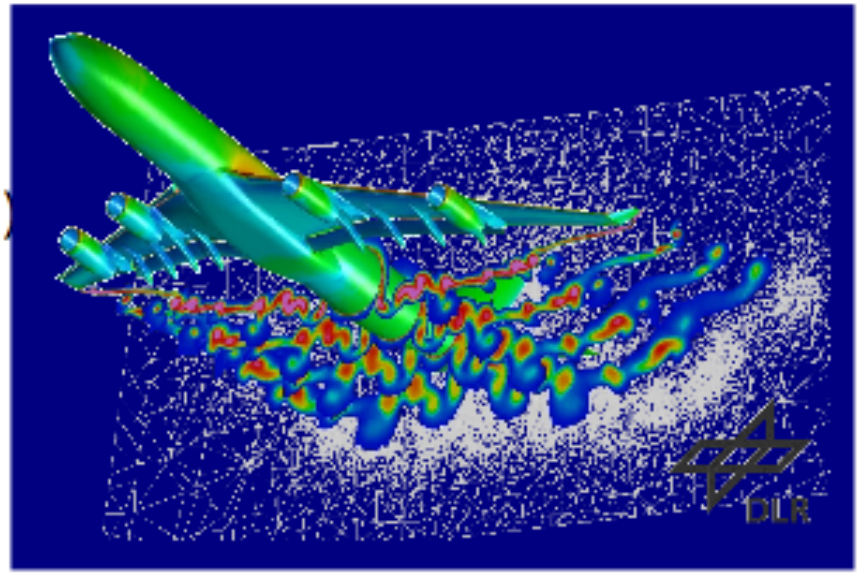

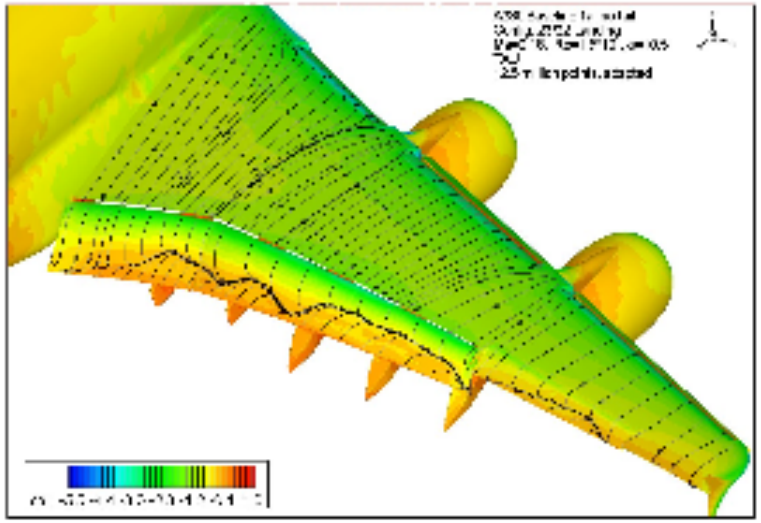

TAU-Code

- unstructured database
- C-code, Python
- portable code, optimized for cache hardware
- high performance on parallel computer

Numerical Flow Simulation

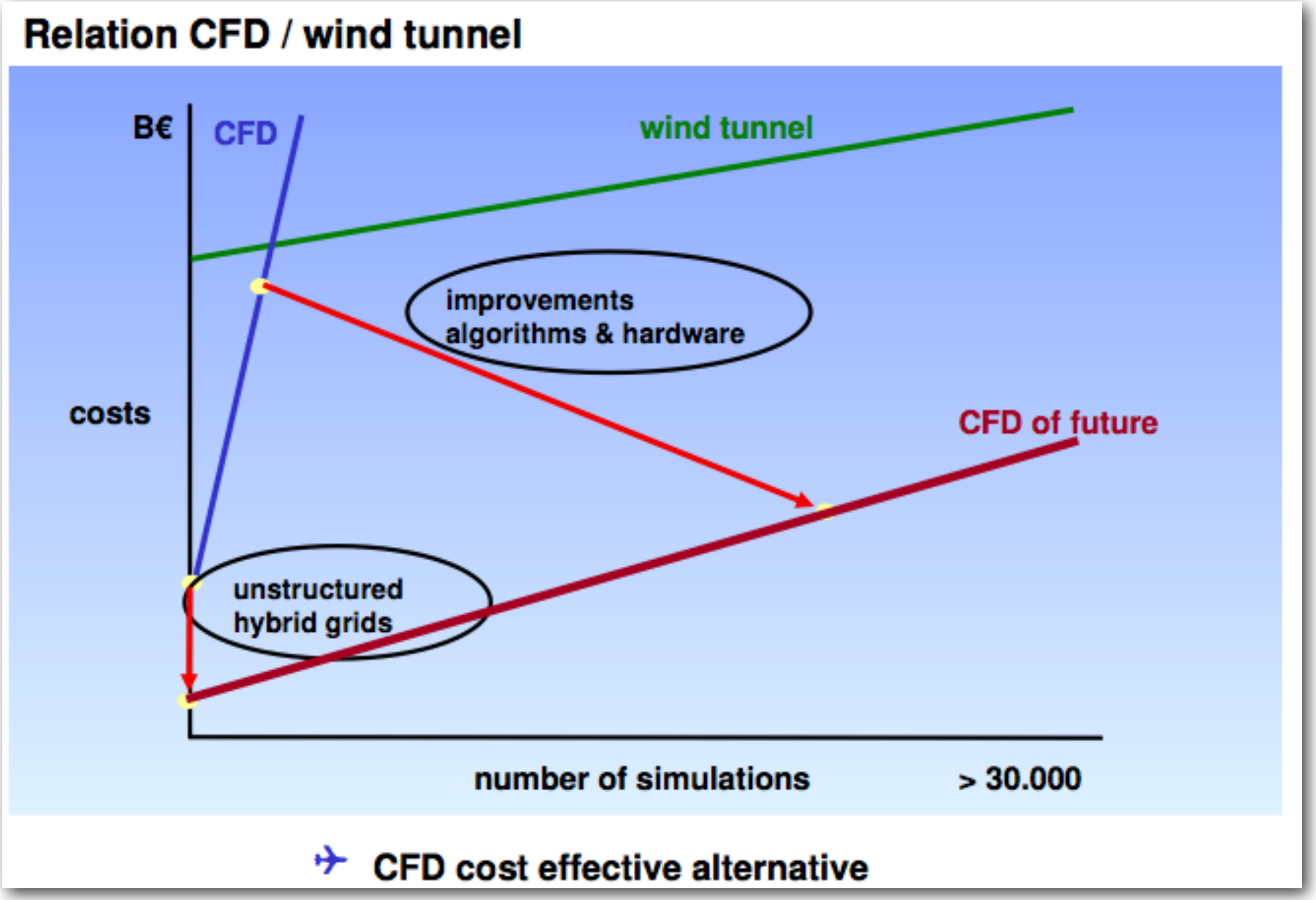

CFD Contribution to A380

Wing Optimization Using SYN107

State of the Art Wing Design Process in 2 Stages, starting from Garabedian-Korn Airfoil and NASA Common Research Model

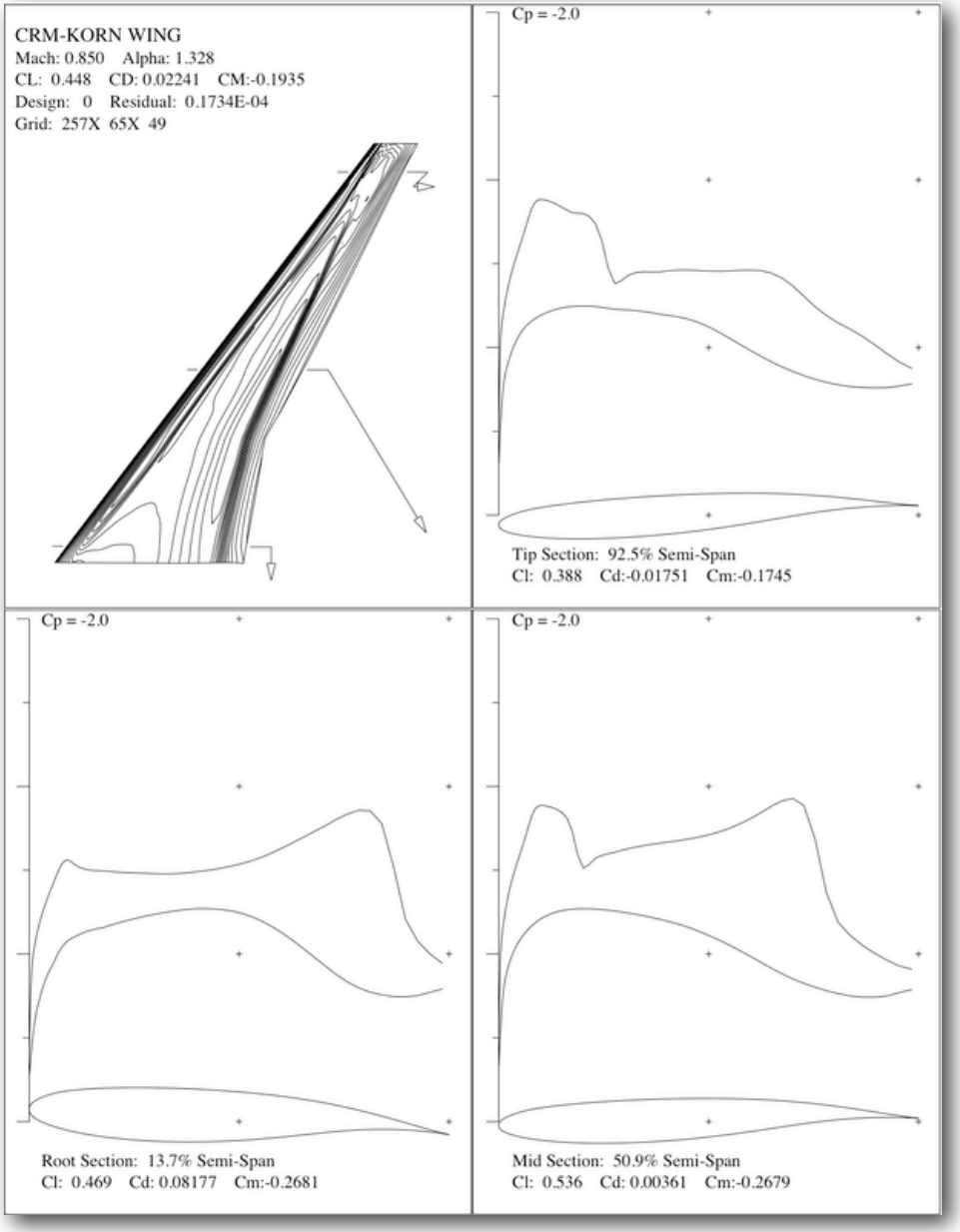

Outline

The Current Status of CFD

- Worldwide commercial and government codes are based on algorithms developed in the '80s and '90s
- These codes can handle complex geometry but are generally limited to 2nd order accuracy
- They cannot handle turbulence without modeling
- Unsteady simulations are very expensive, and questions over accuracy remain

The Future of CFD (?)

CFD has been on a plateau for the past 15 years

- Representations of current state of the art:
  - Formula 1 cars
  - Complete aircrafts
- The majority of current CFD methods are not adequate for vortex dominated and transitional flows:
  - Rotorcraft
  - High-lift systems
  - Formation flying

The Future of CFD

The Future of CFD

The Future of CFD

Large-Eddy Simulation

The number of DoF for an LES of turbulent flow over an airfoil scales as **$Re_c^{1.8}$ (resp. $Re_c^{0.4}$) if the inner layer is resolved (resp. modeled)**

Rapid advances in computer hardware should make LES feasible within the foreseeable future for industrial problems at high Reynolds numbers. To realize this goal requires

- high-order algorithms for unstructured meshes (complex geometries)
- Sub-Grid Scale models applicable to wall bounded flows
- massively parallel implementation

Chapman (1979), AIAA J. 17(12)

Typical Requirements of CFD

Traditional numerical schemes for engineering problems are too dissipative and do not provide sufficient accuracy for LES and DNS

- **Accuracy:** solution must be right
- **Small numerical dissipation:** unsteady flow features
- **Unstructured grids:** complex geometries
- **Numerical flux:** wave propagation problems
- **High resolution capabilities:** transitional and turbulent flows
- **Efficiency:** code parallelism
- ...

A Review of the Literature

Past Research on DG Schemes:

- Modern development of DG schemes for hyperbolic conservation laws stems from the work of Cockburn & Shu [1989a,1989b,1990,1998,2001]

Recent Research:

Attempts to reduce complexity and avoid quadrature:

- Spectral Difference (SD) scheme by Kopriva & Kolias [1996], Liu, Vinokur & Wang [2006]
- Nodal Discontinuous Galerkin (NDG) scheme by Atkins & Shu [1998], Hesthaven & Warburton [2007]
- Flux Reconstruction (FR) scheme by Huynh [2007,2009]

Cockburn, et al. (1989). J. Comput. Phys., 84(1); Cockburn, Shu (1989). Math. Comput., 52; Cockburn, et al. (1990). Math. Comput., 54(190); Cockburn, Shu (1998). J. Comput. Phys., 141; Cockburn, Shu (2001). J. Sci. Comput., 16; Kopriva, Kolias (1996). J. Comput. Phys., 125(1); Liu, et al. (2006). J. Comput. Phys., 216(2); Atkins, Shu (1998). AIAA J., 36(5); Hesthaven, Warburton, (Springer Verlag, 2007); Huynh, (2007). AIAA P., 2007-4079; Huynh, (2009) AIAA P., 2009-403

Outline

Introduction

- **The following presentation emphasizes development of Huynh's FR approach, and energy stability**
- **Energy stability analysis versus Fourier stability analysis**
  - Energy method is more general and rigorous
  - Energy method enables stability proofs for all orders of accuracy
  - Energy method applies to non-uniform meshes
  - *Fourier analysis provides more detailed information about the distribution of dispersive and diffusive errors*
  - *Fourier analysis identifies super accuracy for linear problems*

The Energy Stable FR scheme (ESFR):

- **Until recently, stable FR schemes identified on an ad hoc basis**
- **We have identified a range of correction functions that guarantee linear stability for all orders of accuracy**
- **Achieved by extending Jameson's proof of stability of an SD scheme for the linear advection equation for all orders of accuracy**

The Flux Reconstruction Scheme

The solution is locally represented by Lagrange polynomial of degree $n-1$ on the solution points:

$$u_h = \sum_{j=1}^{n} u_j l_j(x) \qquad f_h^D = \sum_{j=1}^{n} f_j^D l_j(x)$$

The flux is discontinuous and needs to be corrected in a suitable way

$$\Delta_L = \widetilde{f}_L - f_h^D(-1) \qquad \Delta_R = \widetilde{f}_R - f_h^D(1)$$

$$h_L(-1) = 1, \quad h_L(1) = 0 \qquad h_R(1) = 1, \quad h_R(-1) = 0$$

The continuous flux is obtained from the discontinuous counterpart by adding the correction functions of degree n weighted by the flux corrections

$$f_h^C = \sum_{j=1}^{n} f_j^D l_j(x) + h_L(x)\Delta_L + h_R(x)\Delta_R$$

The continuous flux is finally differentiated at the solution points and the solution is advanced in time

$$\frac{\partial u_i}{\partial t} + \left[\sum_{j=1}^{n} f_j^D \frac{\mathrm{d}l_j}{\mathrm{d}x}(x_i) + \Delta_L \frac{\mathrm{d}h_L}{\mathrm{d}x}(x_i) + \Delta_R \frac{\mathrm{d}h_R}{\mathrm{d}x}(x_i) \right] = 0$$

Huynh, (2007). AIAA P., 2007-4079; Huynh, (2009) AIAA P., 2009-403

The FR Scheme Graphically Illustrated

The solution is locally represented by Lagrange polynomial of degree *n*-1 on the *n* solution points:

$$u_h = \sum_{j=1}^{n} u_j l_j(x)$$

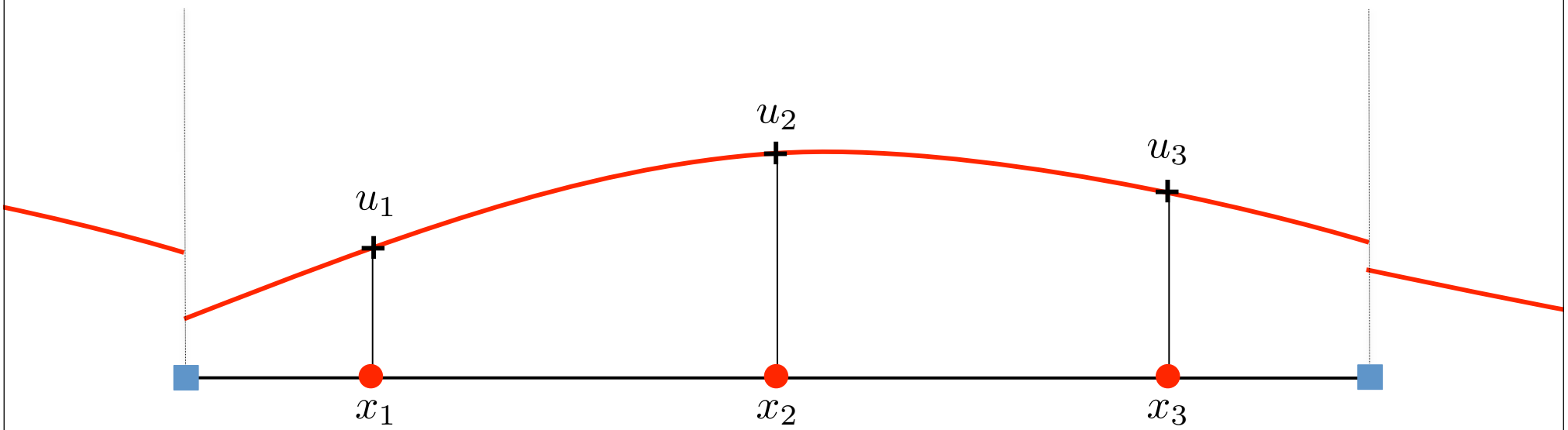

Huynh, (2007). AIAA P., 2007-4079; Huynh, (2009) AIAA P., 2009-403

The FR Scheme Graphically Illustrated

The discontinuous flux is constructed

$$f_h^D = \sum_{j=1}^{n} f_j^D l_j(x)$$

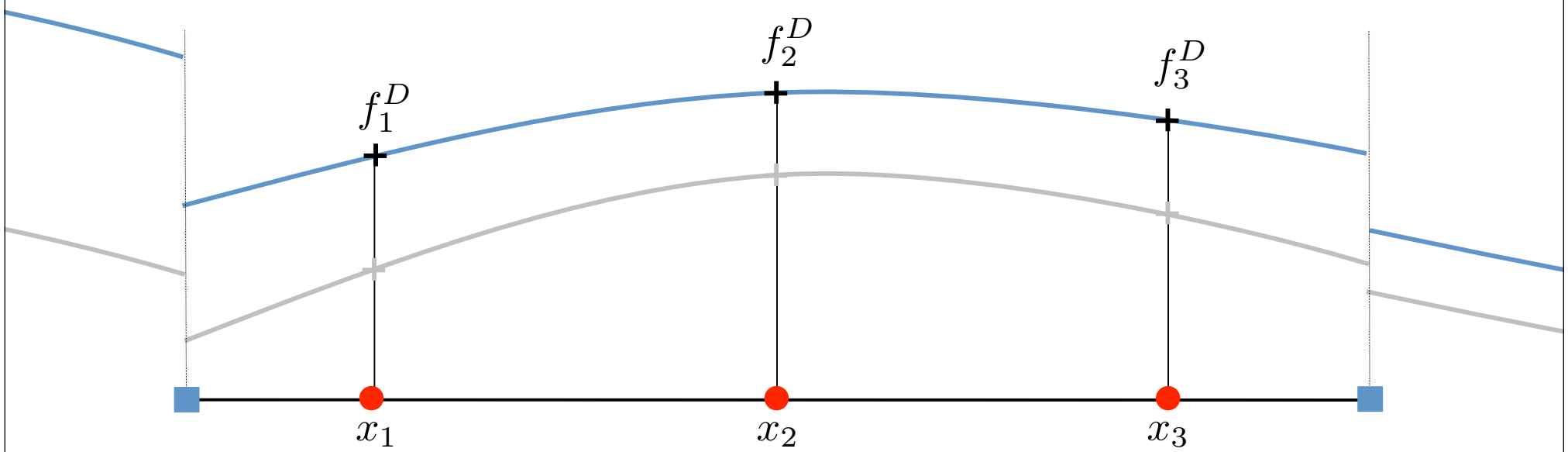

Huynh, (2007). AIAA P., 2007-4079; Huynh, (2009) AIAA P., 2009-403

The FR Scheme Graphically Illustrated

Solution is evaluated at element boundaries

$$u_L = \sum_{j=1}^{n} u_j l_j(-1) \qquad u_R = \sum_{j=1}^{n} u_j l_j(+1)$$

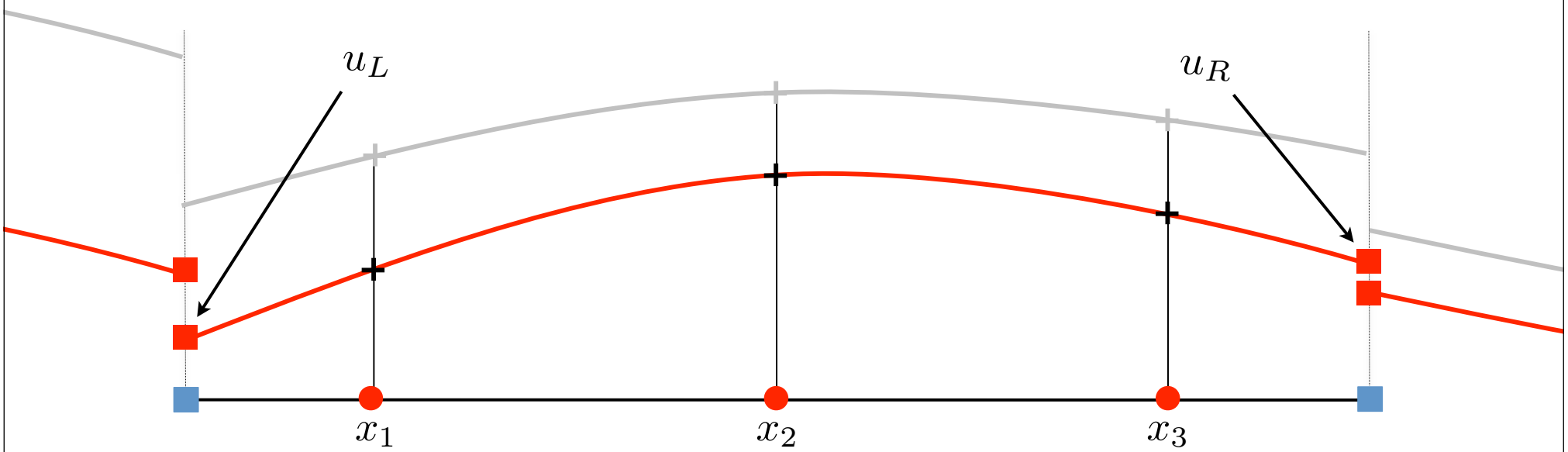

Huynh, (2007). AIAA P., 2007-4079; Huynh, (2009) AIAA P., 2009-403

The FR Scheme Graphically Illustrated

The common interface flux is computed from multiply defined values at each interface (FV-type numerical flux such as approximate Riemann flux)

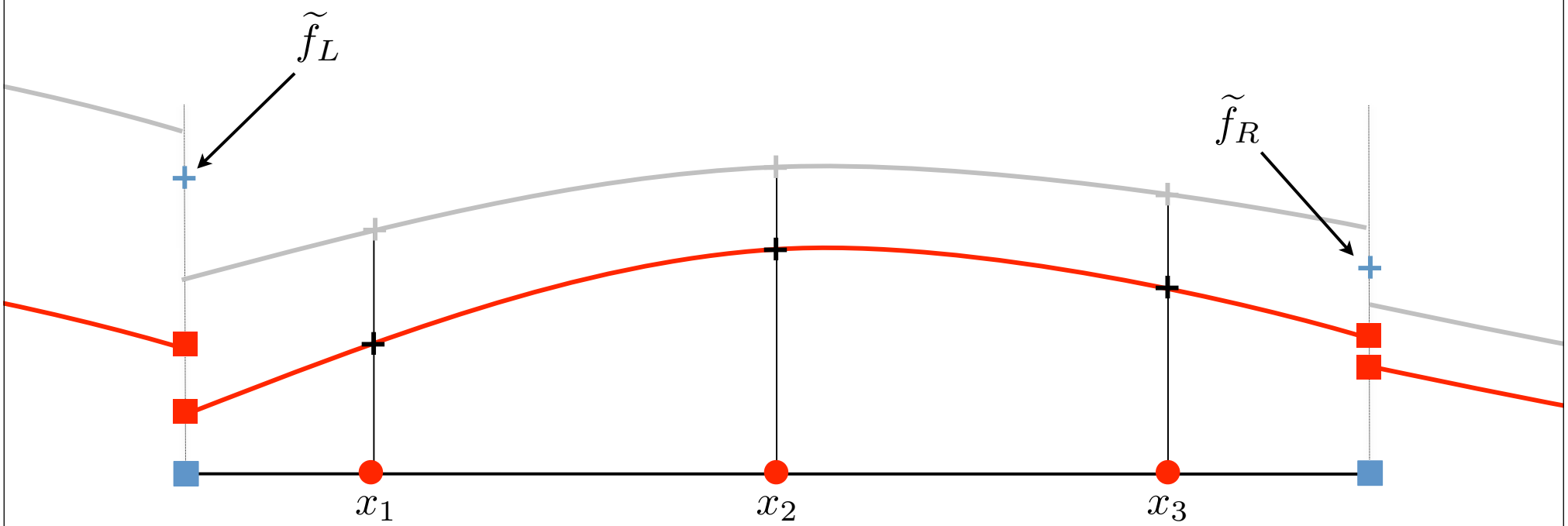

Huynh, (2007). AIAA P., 2007-4079; Huynh, (2009) AIAA P., 2009-403

The FR Scheme Graphically Illustrated

The **common** interface flux is computed from multiply defined values at each interface (FV-type numerical flux such as approximate Riemann flux)

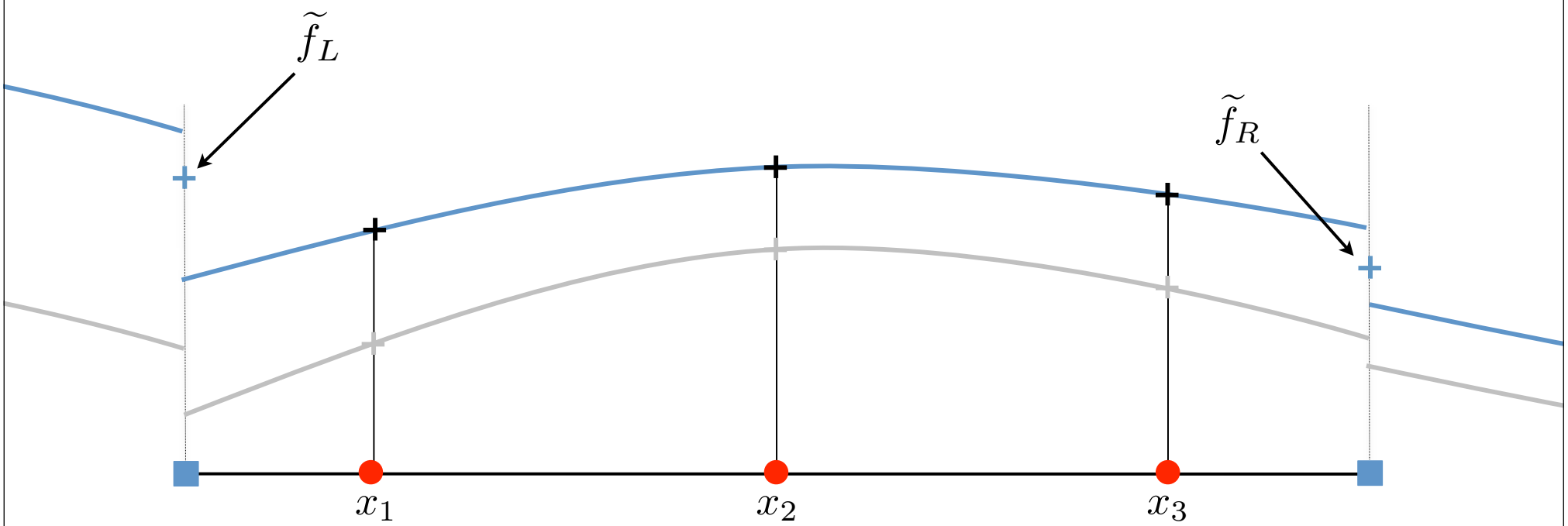

Huynh, (2007). AIAA P., 2007-4079; Huynh, (2009) AIAA P., 2009-403

The FR Scheme Graphically Illustrated

Correction functions of degree *n* are introduced

$$h_L(-1) = 1, \quad h_L(1) = 0$$

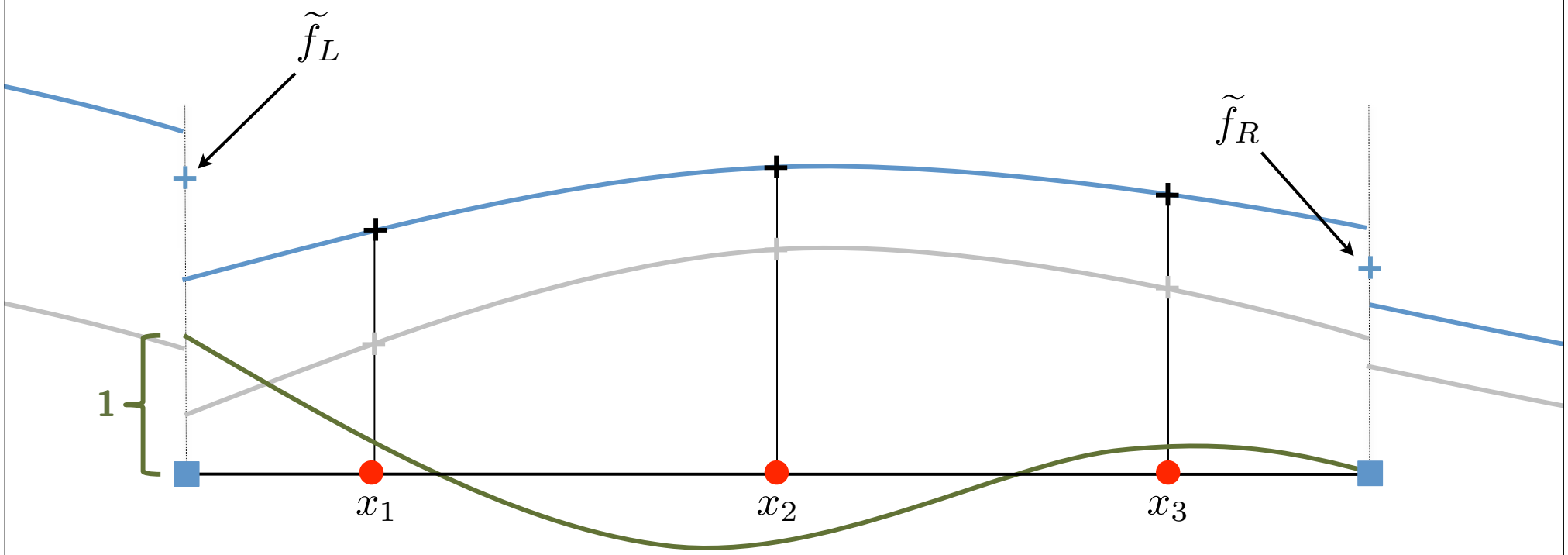

Huynh, (2007). AIAA P., 2007-4079; Huynh, (2009) AIAA P., 2009-403

The FR Scheme Graphically Illustrated

The correction functions are scaled

$$\Delta_L = \widetilde{f}_L - f_h^D(-1)$$

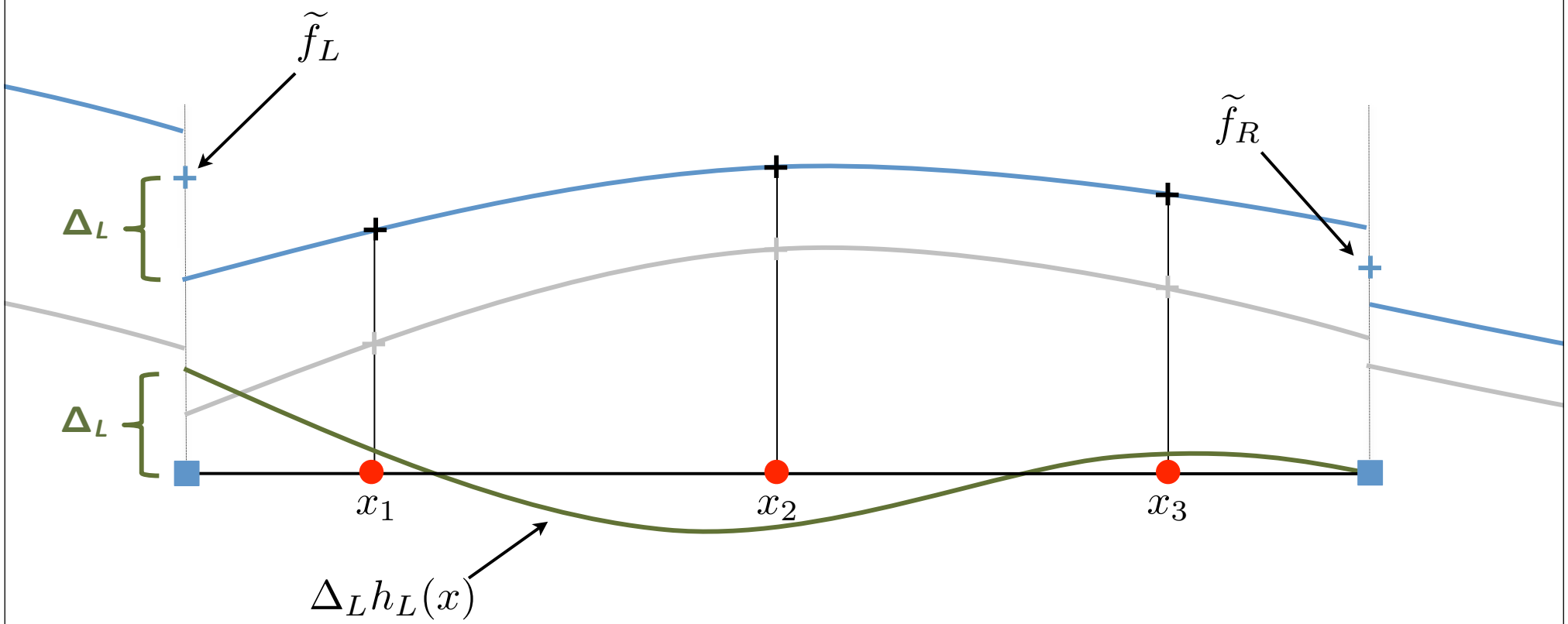

Huynh, (2007). AIAA P., 2007-4079; Huynh, (2009) AIAA P., 2009-403

The FR Scheme Graphically Illustrated

The correction is added to the discontinuous flux

$$f_h^* = \sum_{j=1}^{n} f_j^D l_j(x) + h_L(x)\Delta_L$$

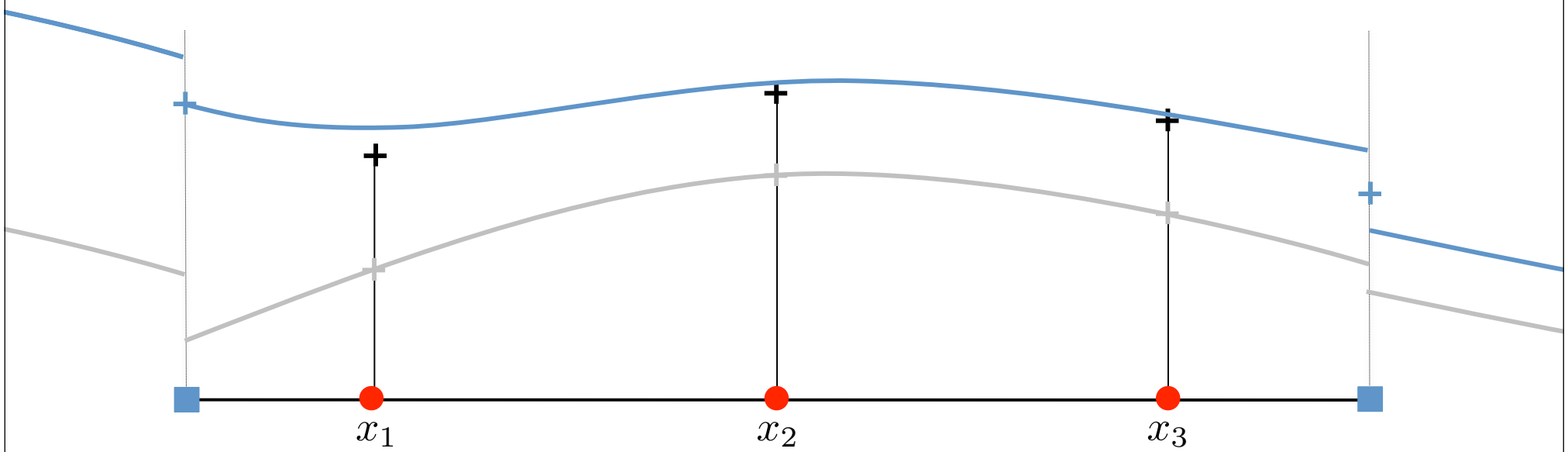

Huynh, (2007). AIAA P., 2007-4079; Huynh, (2009) AIAA P., 2009-403

The FR Scheme Graphically Illustrated

The right boundary is corrected the same way

$$h_R(1) = 1, \quad h_R(-1) = 0$$

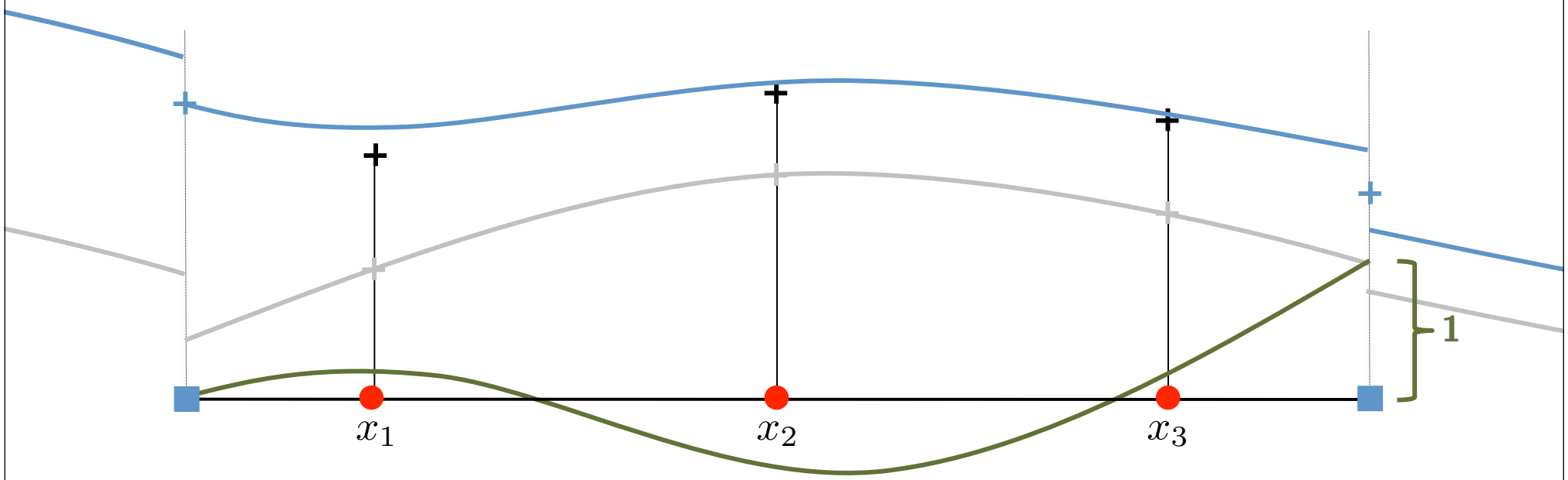

Huynh, (2007). AIAA P., 2007-4079; Huynh, (2009) AIAA P., 2009-403

The FR Scheme Graphically Illustrated

The correction is scaled...

$$\Delta_R = \widetilde{f}_R - f_h^D(+1)$$

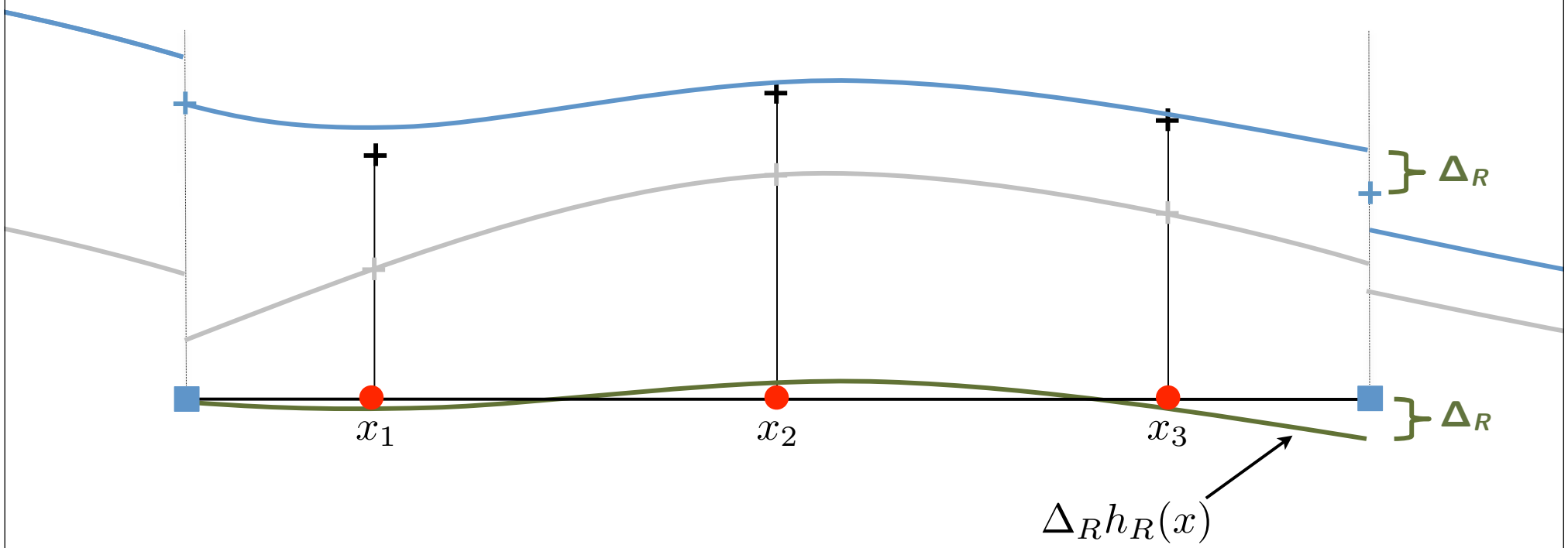

Huynh, (2007). AIAA P., 2007-4079; Huynh, (2009) AIAA P., 2009-403

The FR Scheme Graphically Illustrated

And added to the discontinuous flux

$$f_h^C = \sum_{j=1}^{n} f_j^D l_j(x) + h_L(x)\Delta_L + h_R(x)\Delta_R$$

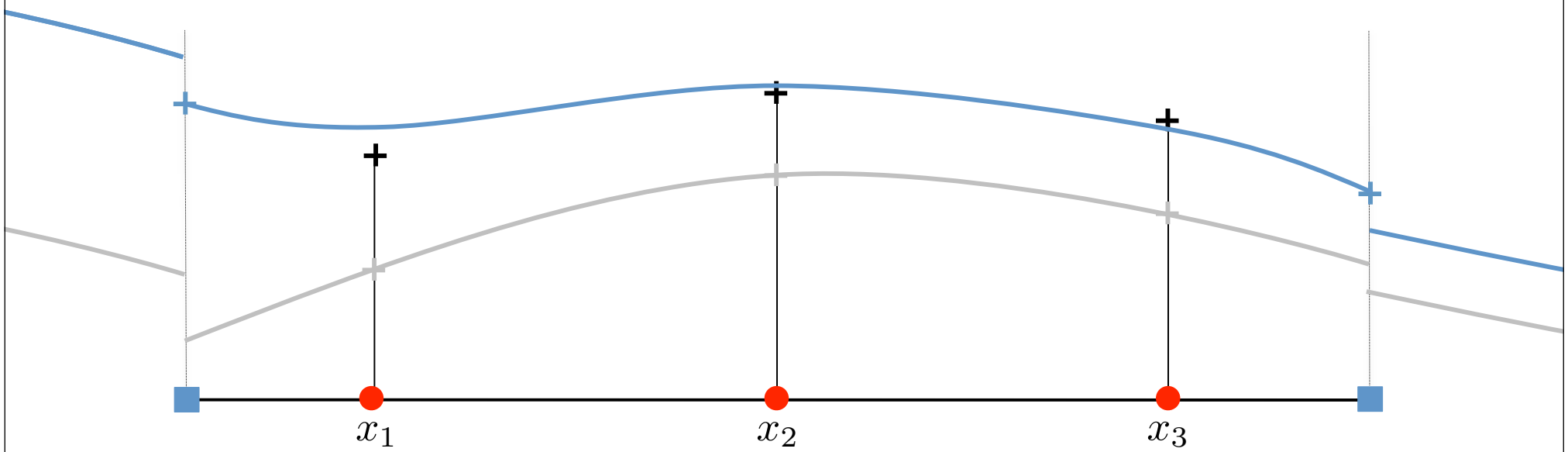

Huynh, (2007). AIAA P., 2007-4079; Huynh, (2009) AIAA P., 2009-403

The FR Scheme Graphically Illustrated

Total approximate continuous flux

$$f_h^C = \sum_{j=1}^{n} f_j^D l_j(x) + h_L(x)\Delta_L + h_R(x)\Delta_R$$

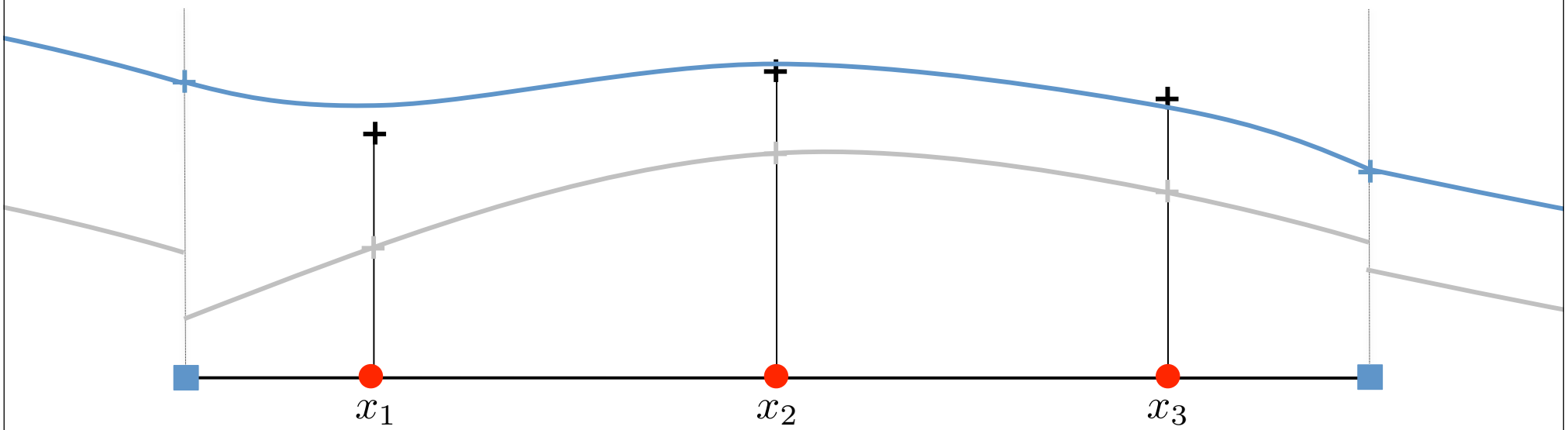

Huynh, (2007). AIAA P., 2007-4079; Huynh, (2009) AIAA P., 2009-403

The FR Scheme Graphically Illustrated

The divergence of the flux is evaluated at the solution points

$$\frac{\partial f^C}{\partial x}(x_i) = \sum_{j=1}^{n} f_j^D \frac{\mathrm{d}l_j}{\mathrm{d}x}(x_i) + \Delta_L \frac{\mathrm{d}h_L}{\mathrm{d}x}(x_i) + \Delta_R \frac{\mathrm{d}h_R}{\mathrm{d}x}(x_i)$$

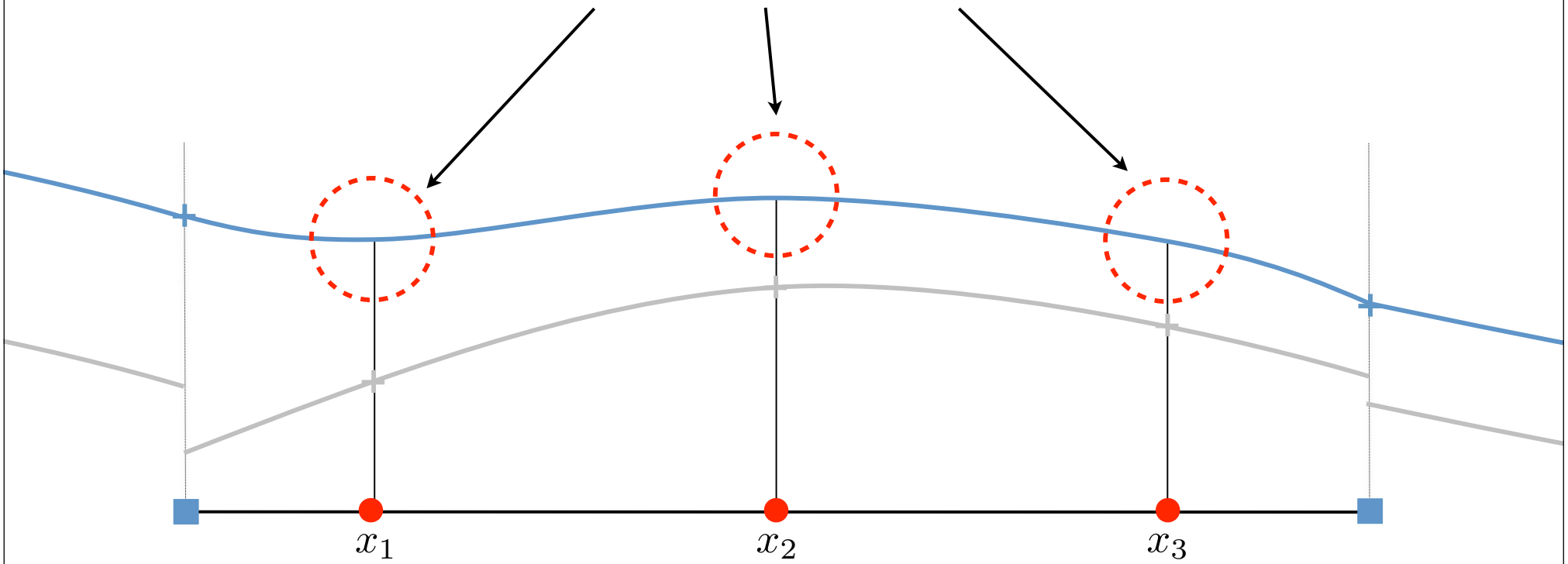

Huynh, (2007). AIAA P., 2007-4079; Huynh, (2009) AIAA P., 2009-403

The FR Scheme Graphically Illustrated

The solution is advanced in time

$$\frac{\partial u_i}{\partial t} + \left[\sum_{j=1}^{n} f_j^D \frac{\mathrm{d}l_j}{\mathrm{d}x}(x_i) + \Delta_L \frac{\mathrm{d}h_L}{\mathrm{d}x}(x_i) + \Delta_R \frac{\mathrm{d}h_R}{\mathrm{d}x}(x_i) \right] = 0$$

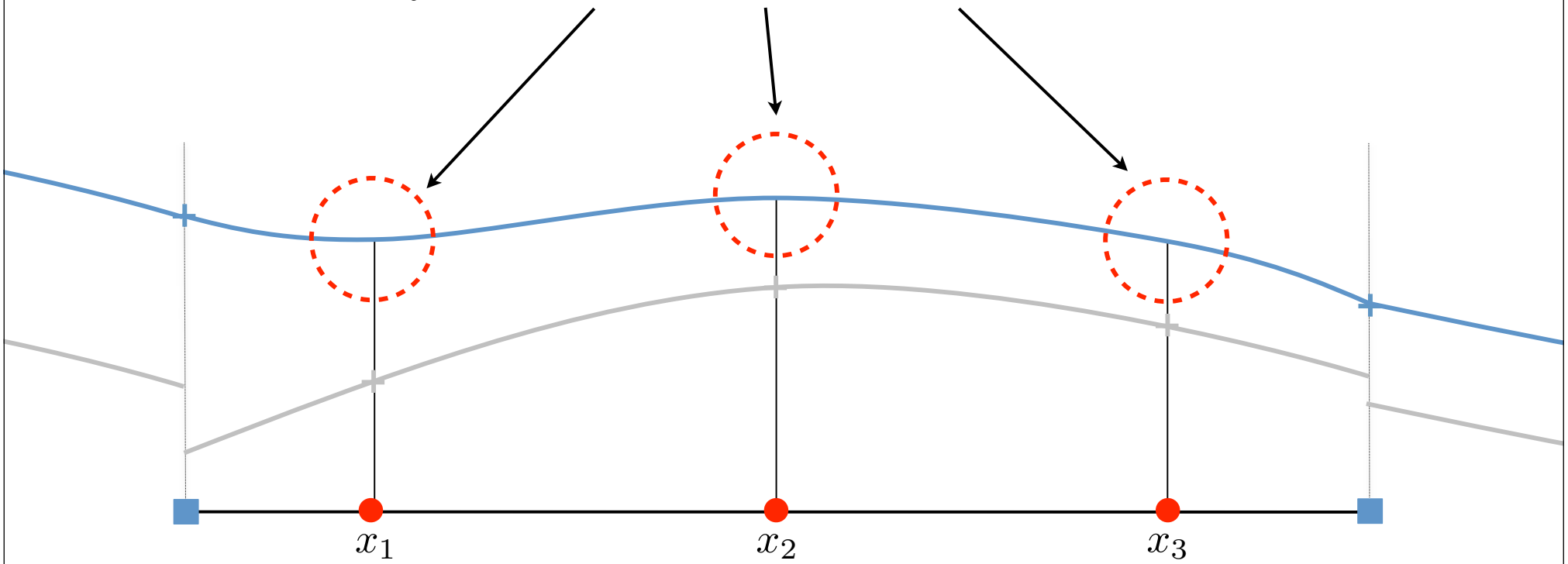

Huynh, (2007). AIAA P., 2007-4079; Huynh, (2009) AIAA P., 2009-403

Energy Stability of the FR Scheme

The FR method defines a family of energy stable schemes in the norm

$$||U^{\delta D}||_{p,2} = \left[\sum_{n=1}^{N} \int_{x_n}^{x_{n+1}} (U_n^{\delta D})^2 + \frac{c}{2}(J_n)^{2p} \left(\frac{\partial^p U_n^{\delta D}}{\partial x^p} \right)^2 \mathrm{d}x \right]^{1/2}$$

The schemes have the form

$$\frac{\partial u_i}{\partial t} + \left[\sum_{j=1}^{n} f_j^D \frac{\mathrm{d}l_j}{\mathrm{d}x}(x_i) + \Delta_L \frac{\mathrm{d}h_L}{\mathrm{d}x}(x_i) + \Delta_R \frac{\mathrm{d}h_R}{\mathrm{d}x}(x_i) \right] = 0$$

where the correction functions in terms of Legendre polynomials are

$$h_L = \frac{(-1)^p}{2} \left[L_p - \left(\frac{\eta_p(c) L_{p-1} + L_{p+1}}{1 + \eta_p(c)} \right) \right]$$

$$h_R = \frac{(+1)^p}{2} \left[L_p + \left(\frac{\eta_p(c) L_{p-1} + L_{p+1}}{1 + \eta_p(c)} \right) \right]$$

with a single parameter c

$$\eta_p(c) = \frac{c(2p+1)(a_p p!)^2}{2}$$

Vincent, et al. (2010). J. Sci. Comput., 47(1); Vincent, et al. (2011). J. Comput. Phys., 230(22)

A Family of Energy Stable Schemes

Accuracy

Allowable Time-Step

Nodal DG:

$$c = 0 \quad \Rightarrow \quad \eta_p = 0$$

$$g_L = \frac{(-1)^p}{2}\left[L_p - L_{p+1}\right], \quad g_R = \frac{(+1)^p}{2}\left[L_p + L_{p+1}\right]$$

Spectral Difference:

$$c = \frac{2p}{(2p+1)(p+1)(a_p p!)^2} \quad \Rightarrow \quad \eta_p = \frac{p}{p+1}$$

$$g_L = \frac{(-1)^p}{2}(1-x)L_p, \quad g_R = \frac{(+1)^p}{2}(1+x)L_p$$

G2 Scheme by Huynh [2007]:

$$c = \frac{2(p+1)}{(2p+1)p(a_p p!)^2} \quad \Rightarrow \quad \eta_p = \frac{p+1}{p}$$

$$g_L = \frac{(-1)^p}{2}\left[L_p - \frac{(p+1)L_{p-1} + pL_{p+1}}{2p+1}\right], \quad g_R = \frac{(+1)^p}{2}\left[L_p + \frac{(p+1)L_{p-1} + pL_{p+1}}{2p+1}\right]$$

Recent Developments and Issues in the FR Approach

- ESFR schemes have been extended to triangles (Castonguay et al. 2011) and tetrahedra (Williams et al. 2013) with proofs for advection/diffusion
- In practice they have proved successful for quadrilateral and hexahedral elements with a tensor product formulation, but so far there is a stability proof only for the nodal DG case (Jameson 2011)
- A general hybrid grid would require pyramid elements for which further research is needed (Jameson 2011)
- Nonlinear stability is improved by the best choice of quadrature points, but additional filtering may be needed

Castonguay, et al. (2011)., Journal of Scientific Computing, DOI:10.1007/s10915-011-9505-3; Williams, et al. (2013)., Publication pending; Jameson, (2011) AIAA P. 2011-3226

Recent Developments and Issues in the FR Approach

- The stability proofs have been developed for semi-discrete schemes, and carry over to fully discrete schemes only in the case of an implicit time-stepping scheme of Crank-Nicolson type (Jameson, 2011)
- An FR formulation for space-time elements remains to be developed
- Further research on shock capturing methods is needed, particularly for moving shocks
- In the case of steady-state problems convergence is excessively slow. Further work on multi h-p schemes is needed, and also on iterative methods and preconditioners for implicit time-stepping schemes

Jameson, (2011) AIAA P. 2011-3226

Outline

Numerical Dissipation

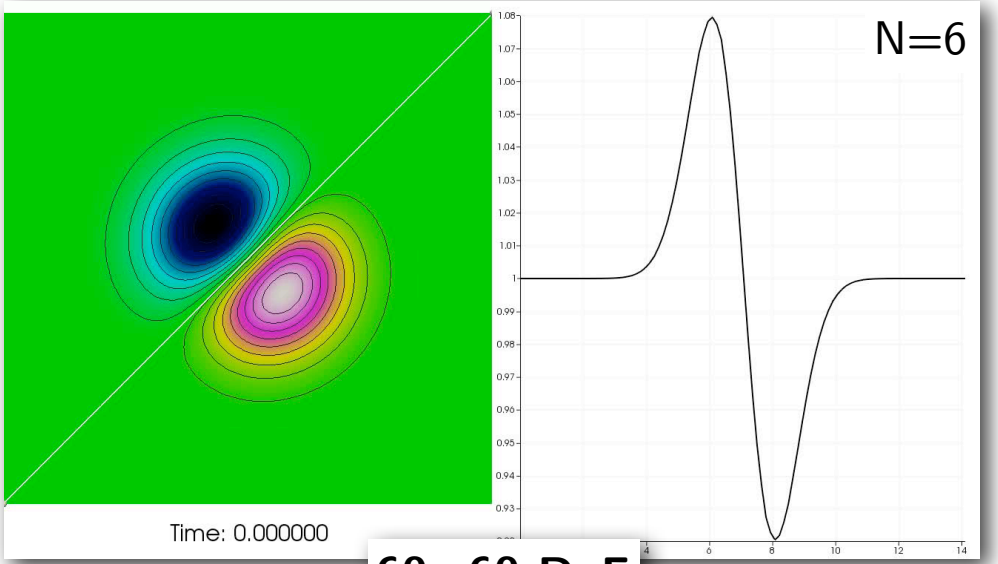

60×60 DoF

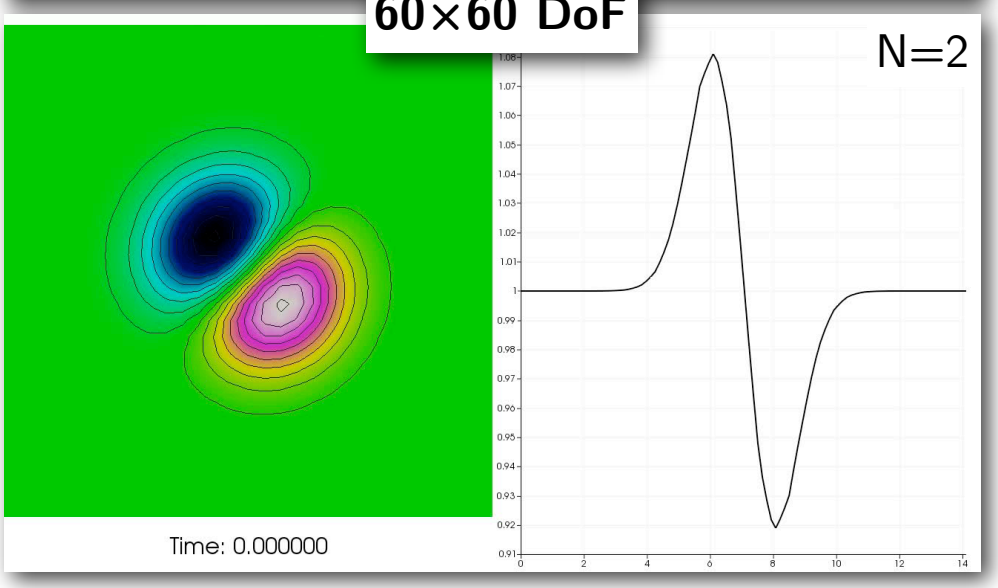

Temporal Mixing-Layer

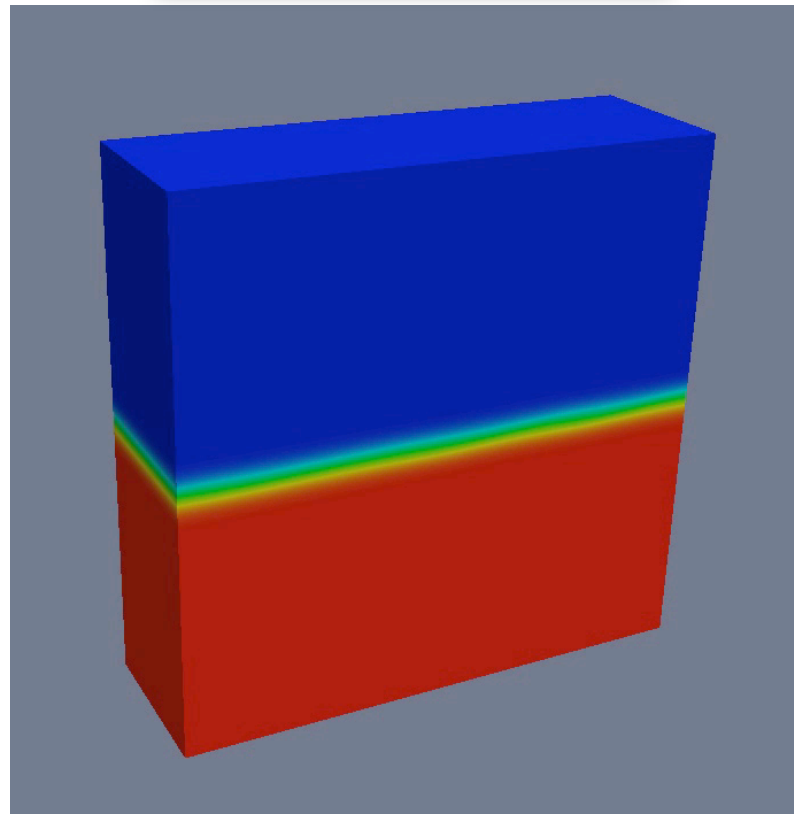

N=5: 100×200×10 DoF

Numerical Dissipation

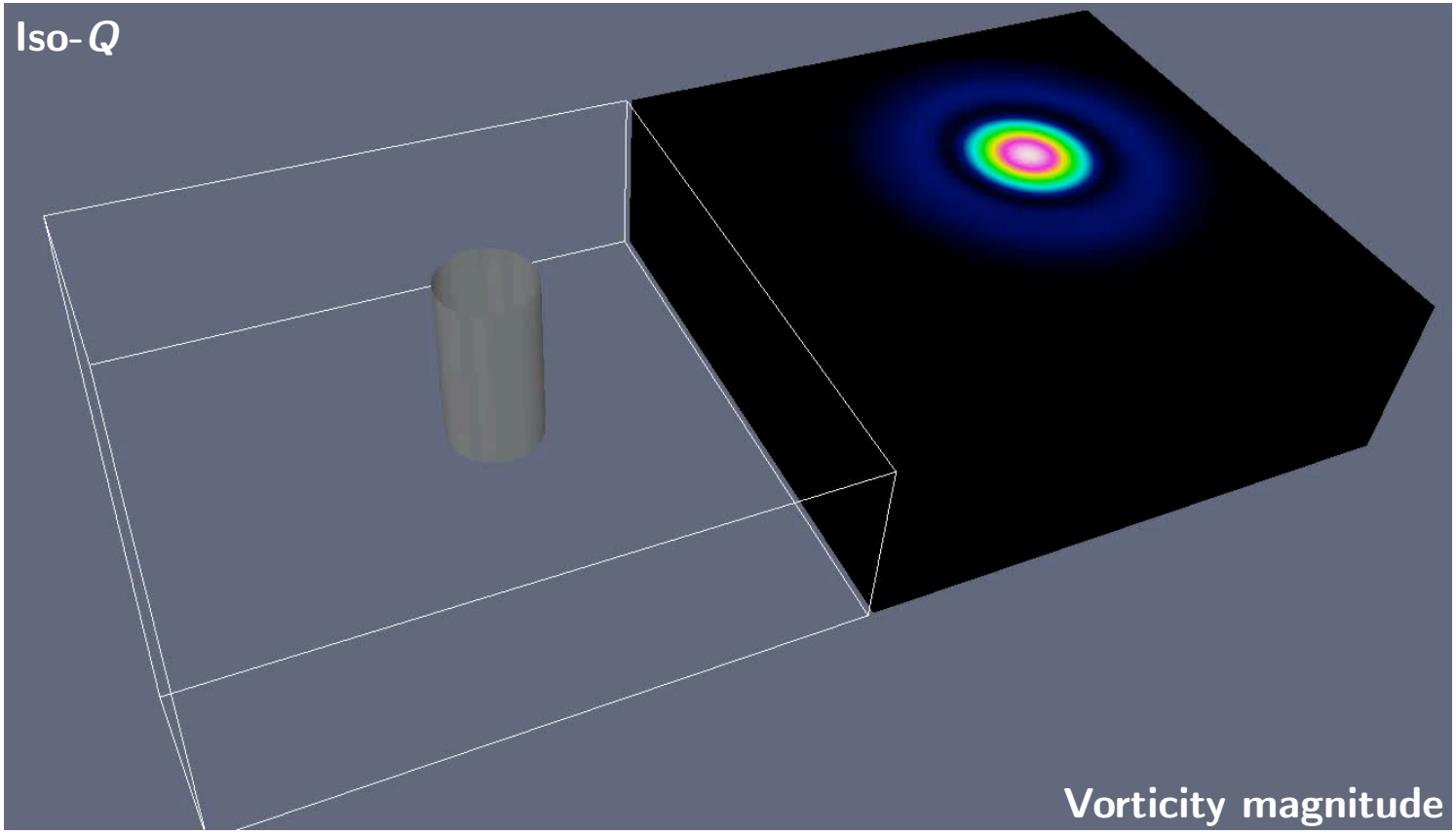

N=6, 60×60×12 DoF

High-Order Boundaries

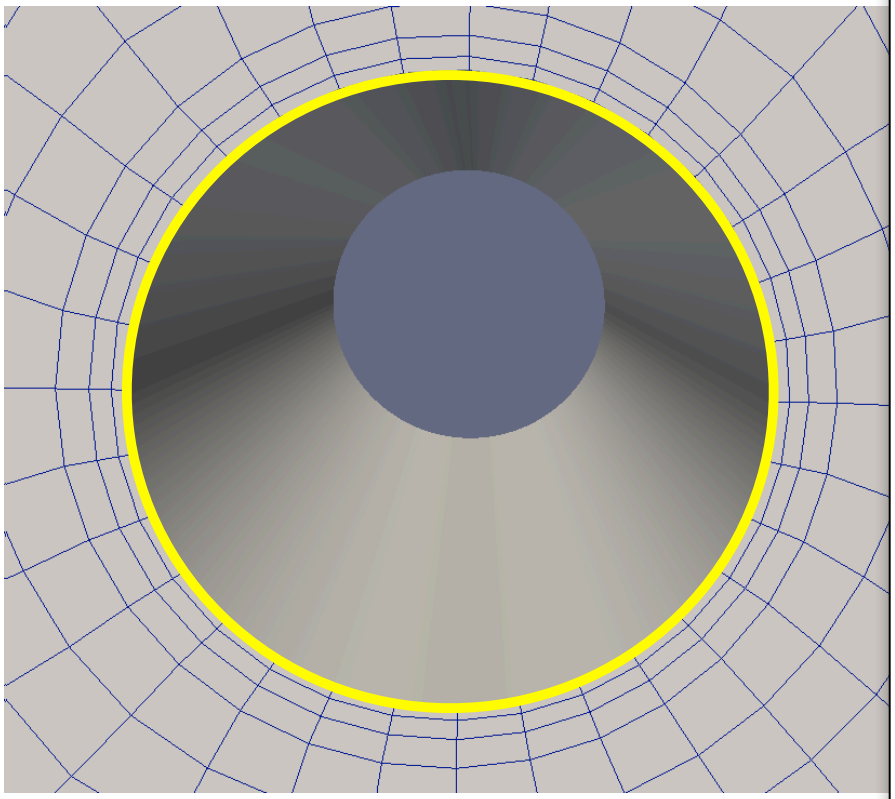

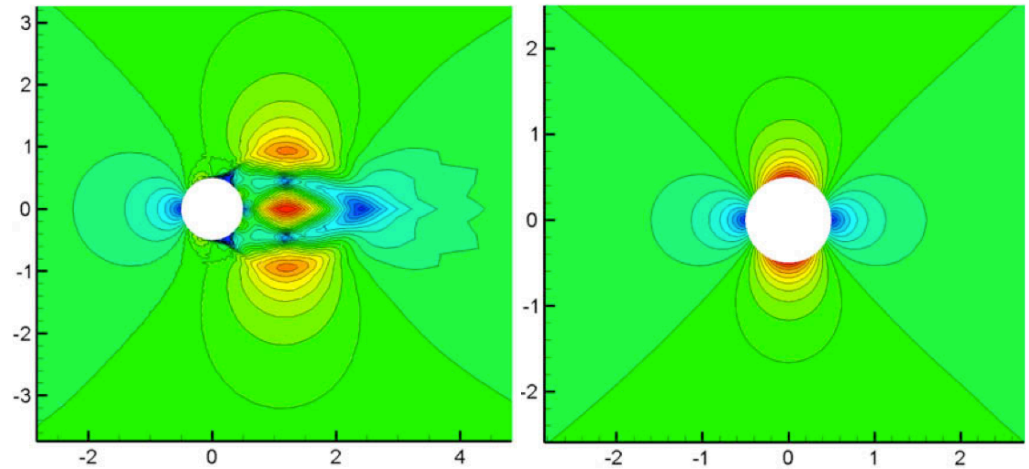

Cylinder: N=4, 32×32, linear *vs.* cubic

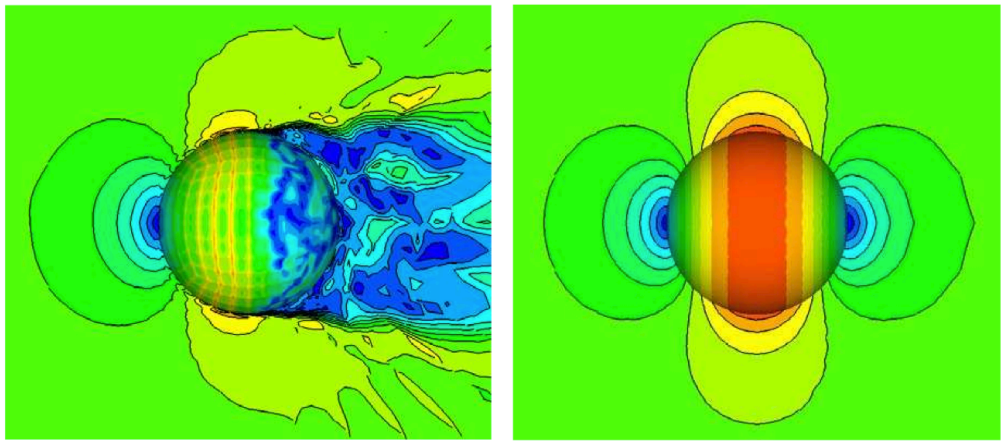

Sphere: N=3, linear *vs.* quadratic

Liang, *et al.* (2009). Comput. Struct., 87; Sun, *et al.* (2007). Commun. Comput. Phys., 2(2)

Transitional Flow over SD7003 Airfoil

	Freestream Turbulence	Separation x_{sep}/c	Transition x_{tr}/c	Reattach. x_r/c
Radespiel et al.	0.08%	0.30	0.53	0.64
Ol et al.	0.10%	0.18	0.47	0.58
Galbraith Visbal	0%	0.23	0.55	0.65
Uranga et al.	0%	0.23	0.51	0.60
Present ILES*	**0%**	**0.23**	**0.53**	**0.64**

Experiments in green

SD scheme, N=4

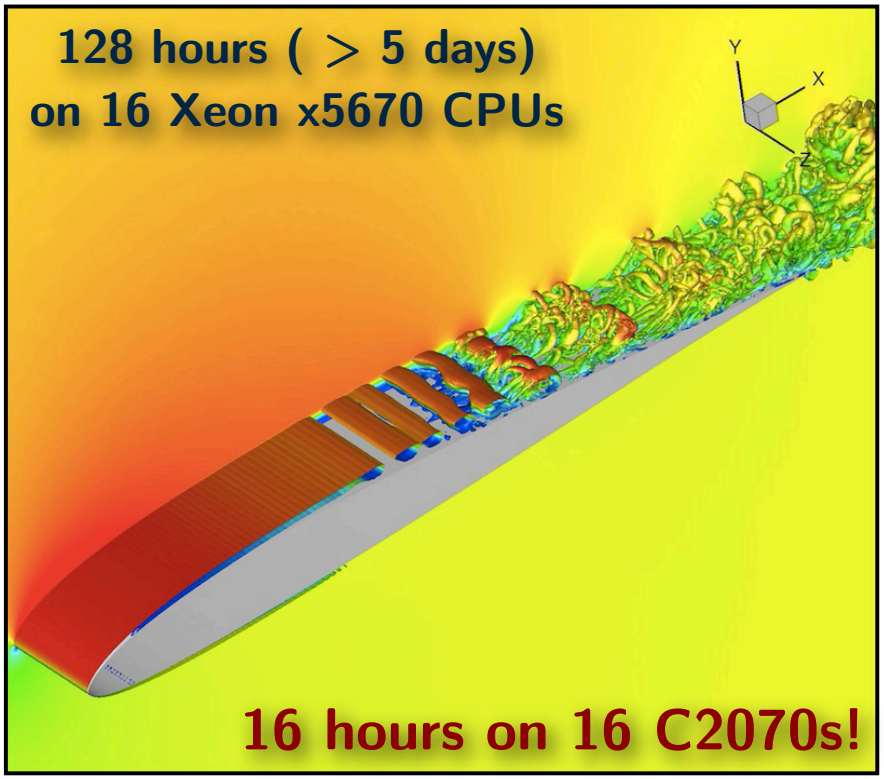

Iso-Q colored by Ma

Re=6×10^4, AoA=4°, 2.2×10^7 DoF

***1.7×10^6 DoF**

Castonguay, et al. (2010). AIAA P., 2010-4626; Radespiel, et al. (2007). AIAA J., 45(6); Ol, et al. (2005). AIAA P., 2005-5149; Galbraith, Visbal (2008). AIAA P., 2008-225; Uranga, et al. (2009). AIAA P., 2009-4131;

Study of Flapping Wing Sections

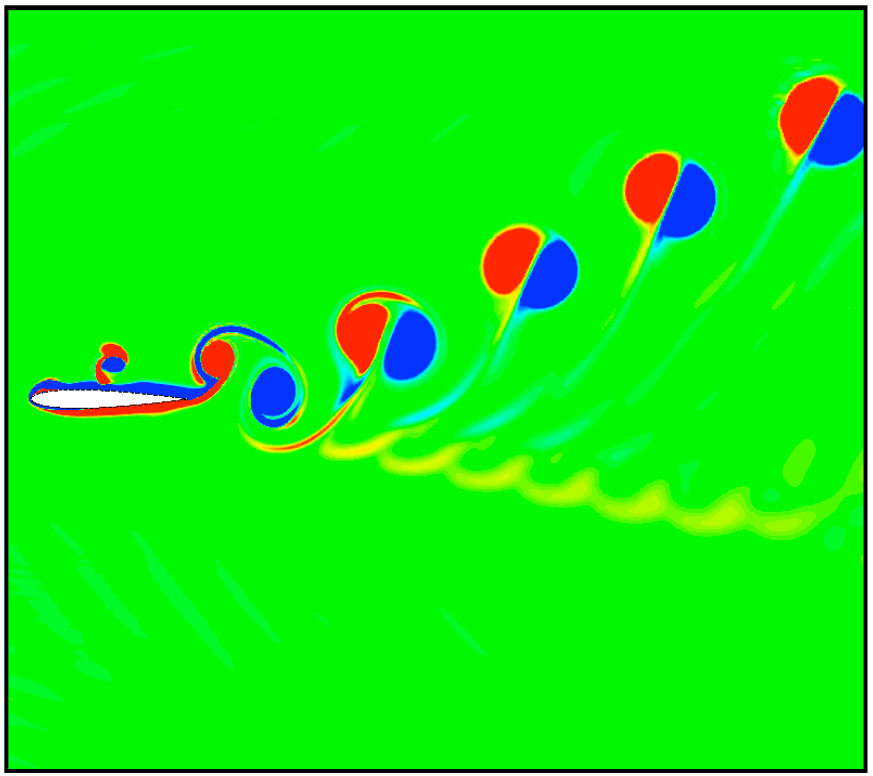

SD, 2D, N=5 on deforming grid

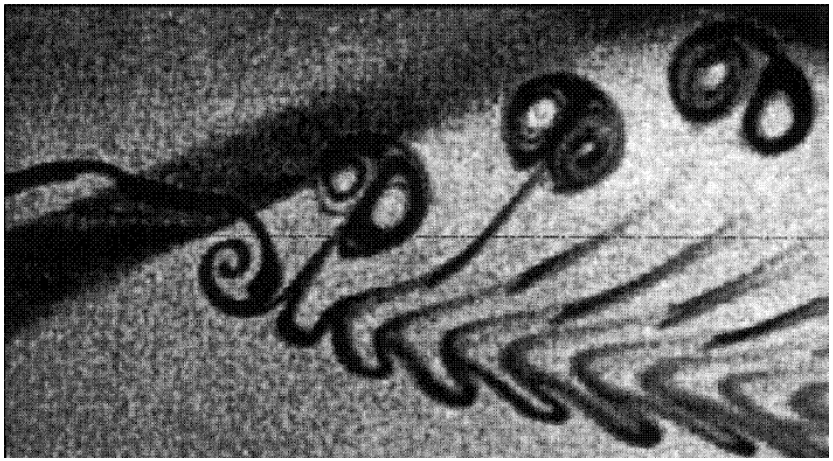

Experiment (Jones, et al.)

NACA0012, Re=1850, Ma=0.2,
St=1.5, ω=2.46, h=0.12c

Jones, et al. (1998). AIAA J., 36(7)

Outline

Explicit Filtering in the SD Element

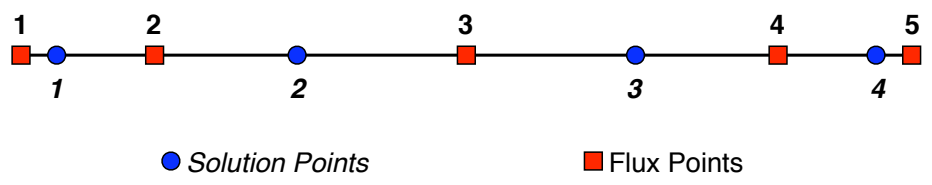

1D element

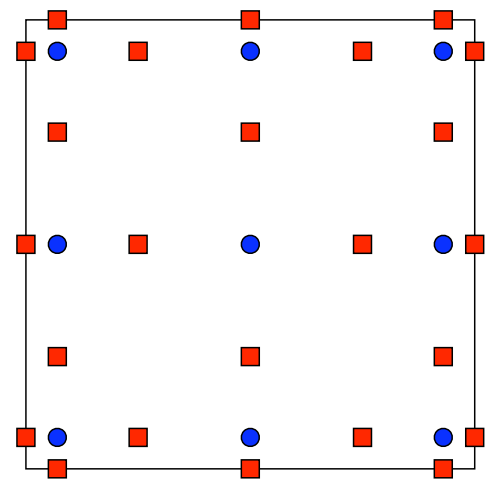

2D element

Key issues:

- non-uniform and staggered distribution of points
- the filter stencil shall not lie across elements
- filter width shall be prescribed and constant

Filtering Strategy:

1. The filtered solution is computed at solution points
2. The SGS model term is evaluated at solution points
3. The SGS model term is extrapolated at flux points via Lagrange basis

Discrete Filtering Operators

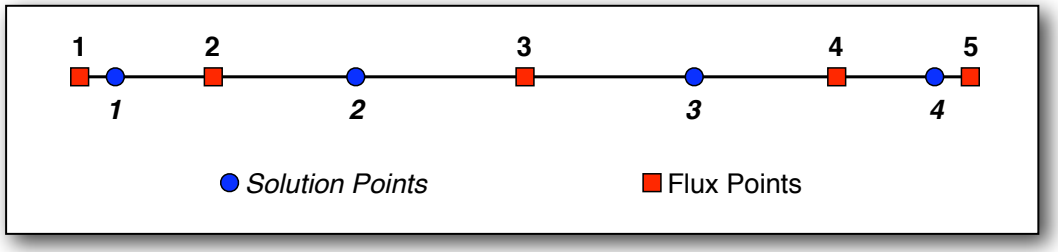

The filtering operator for the 1D standard element is defined as

$$\overline{\phi}_s = \sum_{i=1}^{N} w_i^s \phi_i, \quad (s = 1, \ldots, N)$$

The kernel of the above discrete filter can be written as

$$\widehat{G}_s(k) = \sum_{i=1}^{N} w_i^s \exp(-\mathrm{j}\beta_i^s k\Delta), \quad \text{with} \quad \beta_i^s = \frac{\xi_i - \xi_s}{\Delta}$$

Δ=1/N is assumed to be the actual resolution within the SD element

Vasilyev, et al. (1998). J. Comput. Phys. 146(1); Berland, et al. (2007). J. Comput. Phys. 224(2); Sagaut, Grohens (1999). Int. J. Numer. Meth. Fl. 31(8)

The Restriction-Prolongation Filter

Sharp cutoff in modal space:

The solution is first projected on a lower order polynomial (**restriction** step) and then extrapolated back to the original solution points (**prolongation** step)

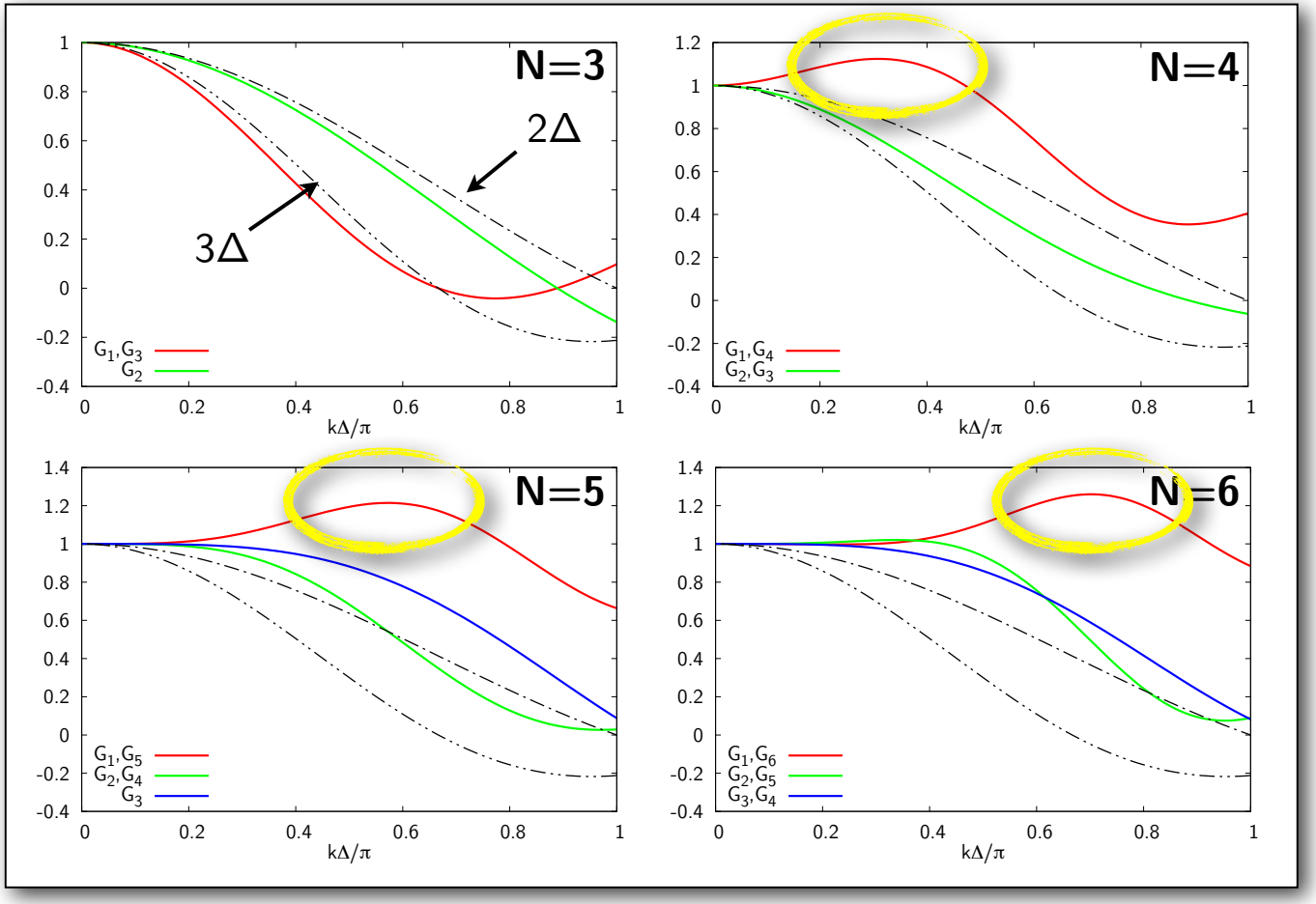

Premasuthan, et al. (2009). AIAA P., 2009-3785

Discrete Filters by Gauss Quadrature

Gauss-Legendre quadrature points:

- The discrete filter is obtained by analytical integration of a selected filter kernel
- Cutoff is enforced iteratively by checking the filter's 2nd moment in physical space

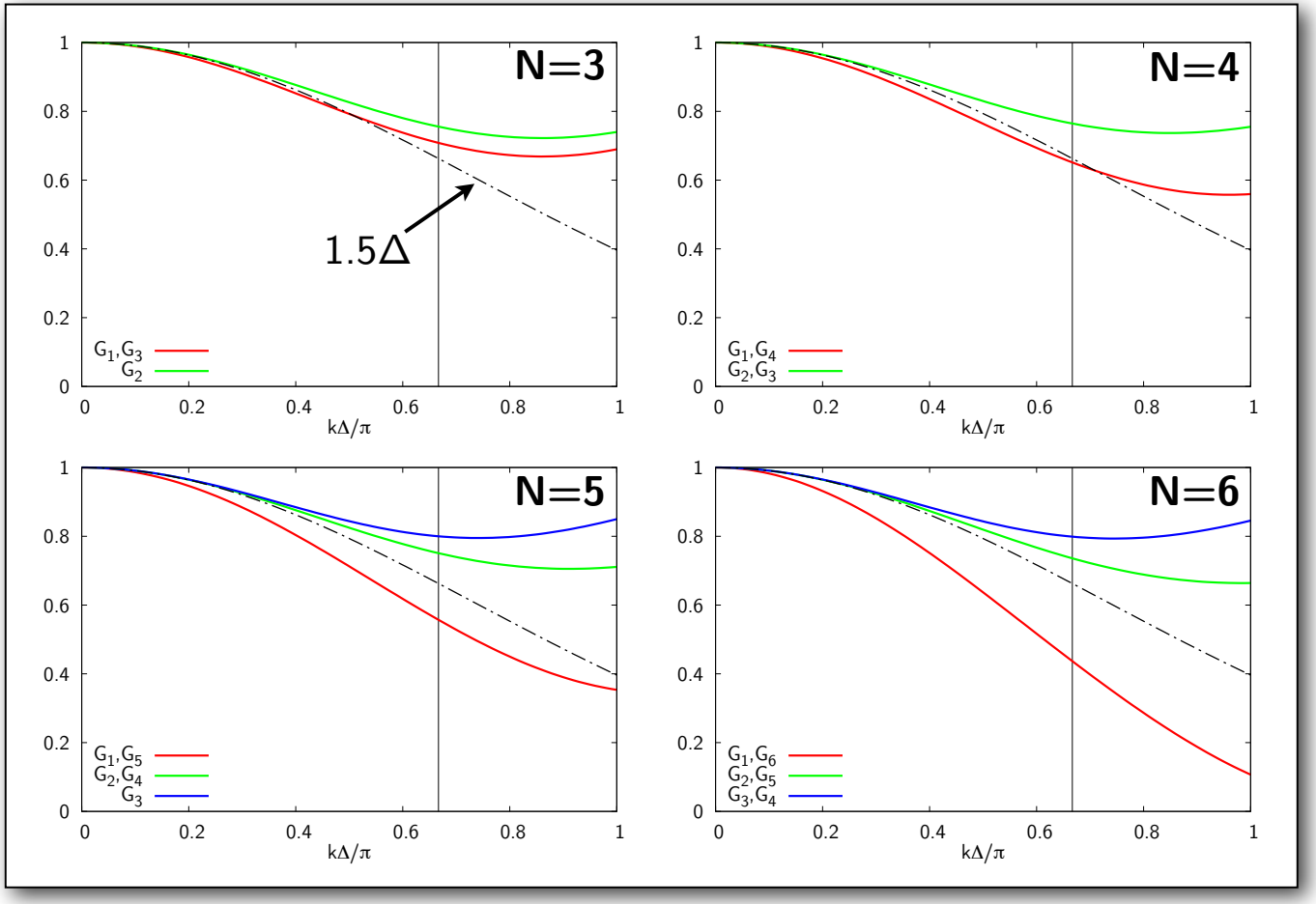

Lodato, Castonguay, Jameson (in preparation)

Discrete Filters for Arbitrary Points

Generalized method of Vasilyev et al. (1998):

- Value and slope at cutoff are enforced using a selected filter kernel (2)
- Higher moments are set to zero (N-3) + preservation of constant variable (1)

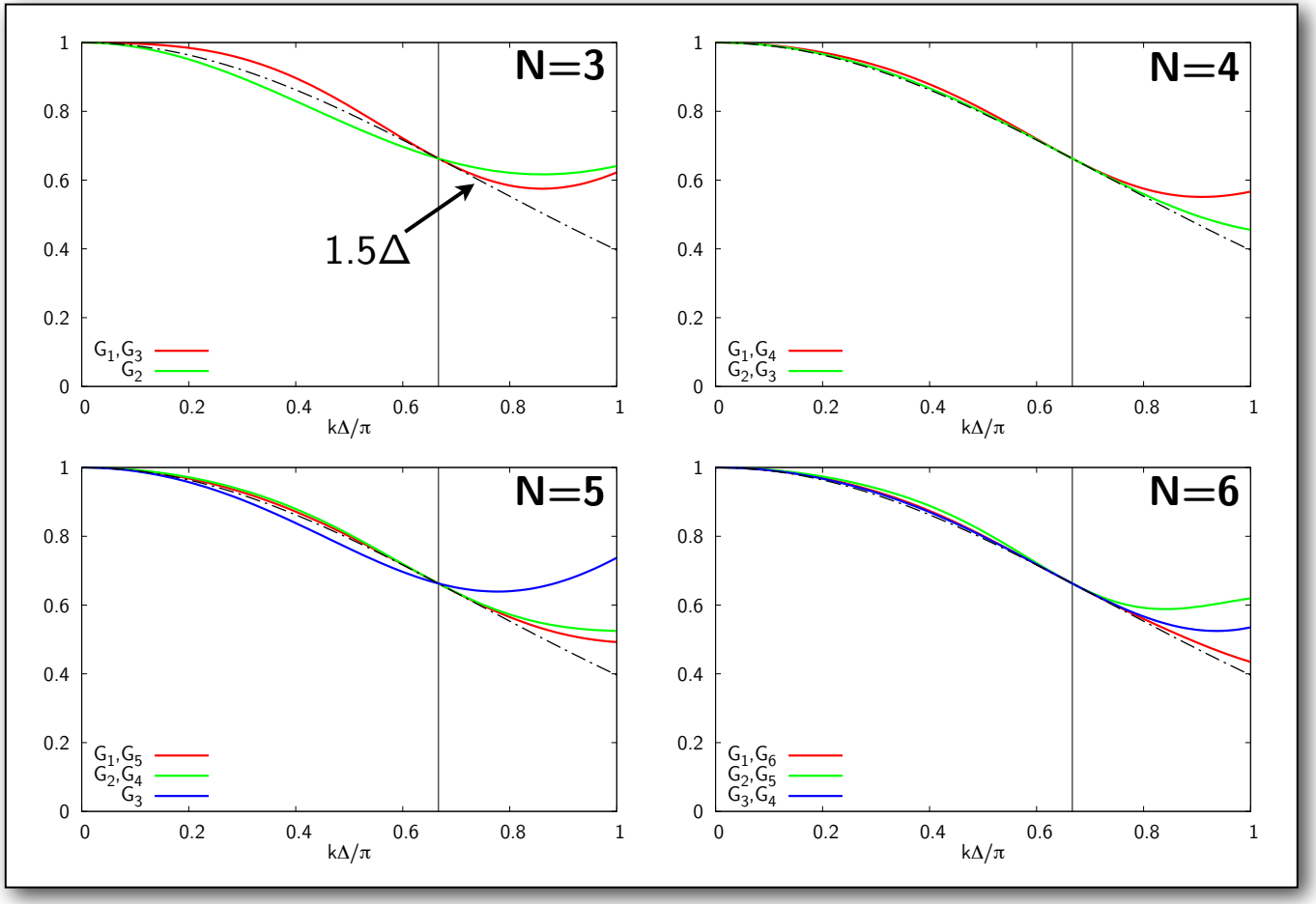

Lodato, Castonguay, Jameson (2011), CTR Annual Research Briefs; Vasilyev et al. (1998), J. Comput. Phys., 146(1)

Outline

Wall-Resolved Turbulent Channel Flow

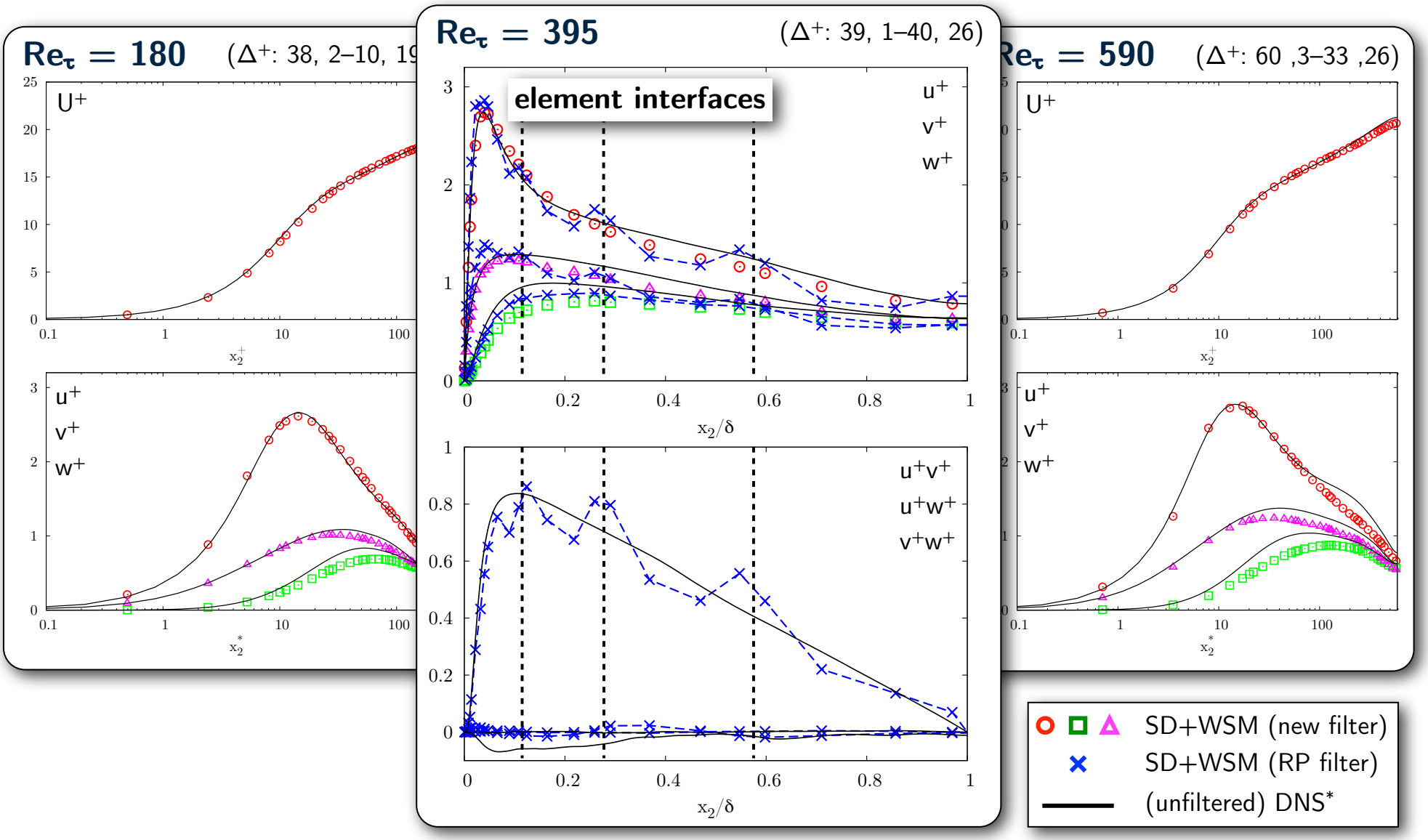

*Moser, et al. (1999). Phys. Fluids, 11(4); Lodato, et al. (2009). Phys. Fluids, 21(3); Premasuthan, et al. (2009). AIAA P., 2009-3785

Wall-Resolved Turbulent Channel Flow

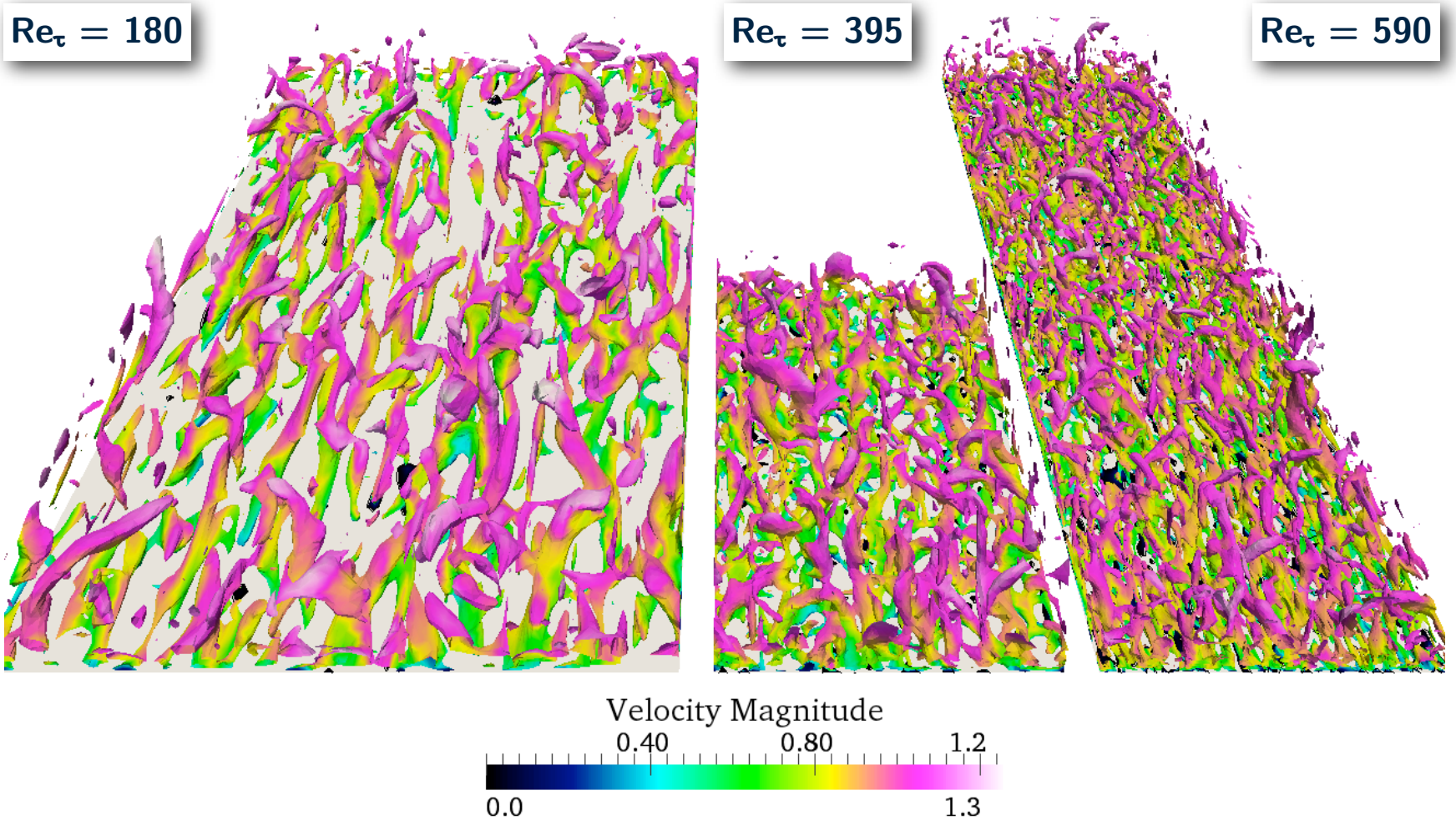

Lodato, Castonguay, Jameson (2011), CTR Annual Research Briefs; Lodato, et al. (2009). Phys. Fluids, 21(3)

A Wall-Modeling Strategy

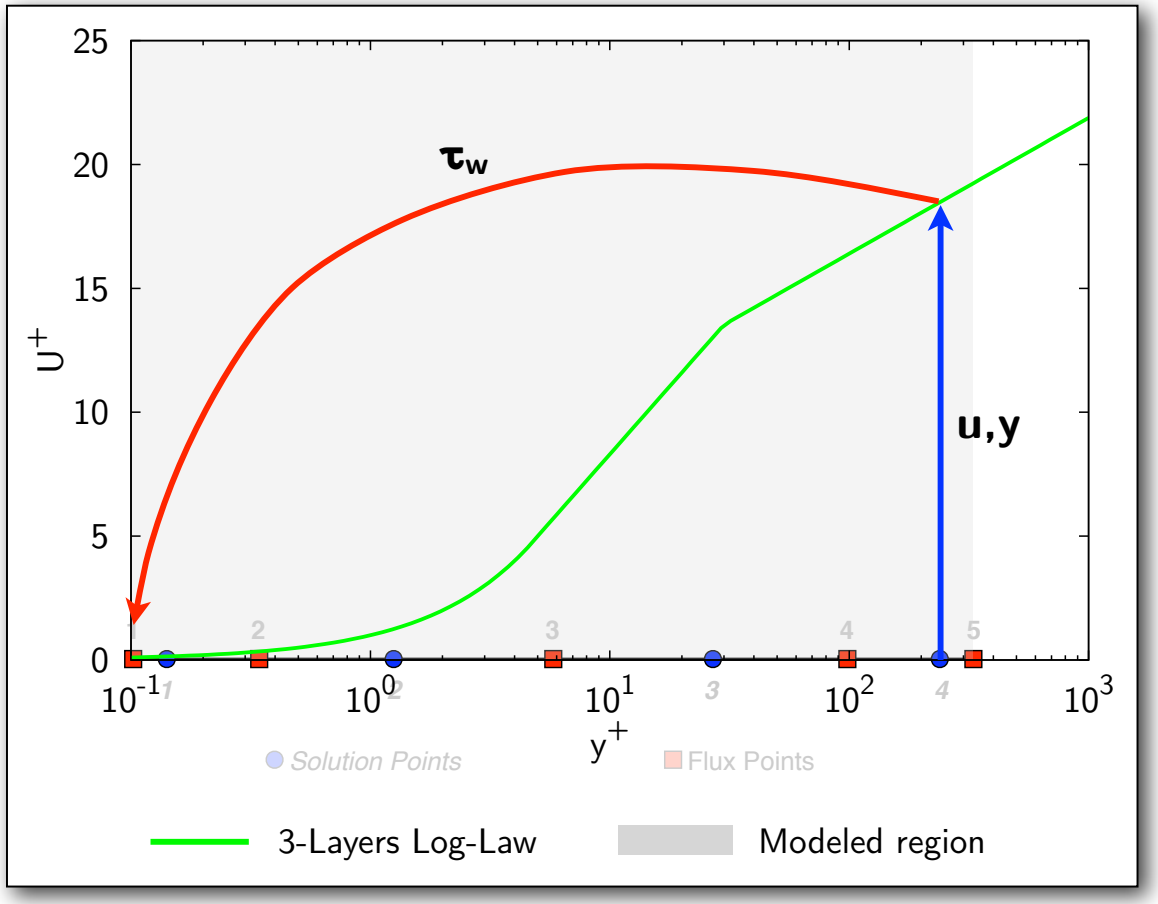

Breuer and Rodi (1996)

Wall-Modeled Turbulent Channel Flow

$Re_\tau = 590$ (Δ^+: 58, 24–47, 58)

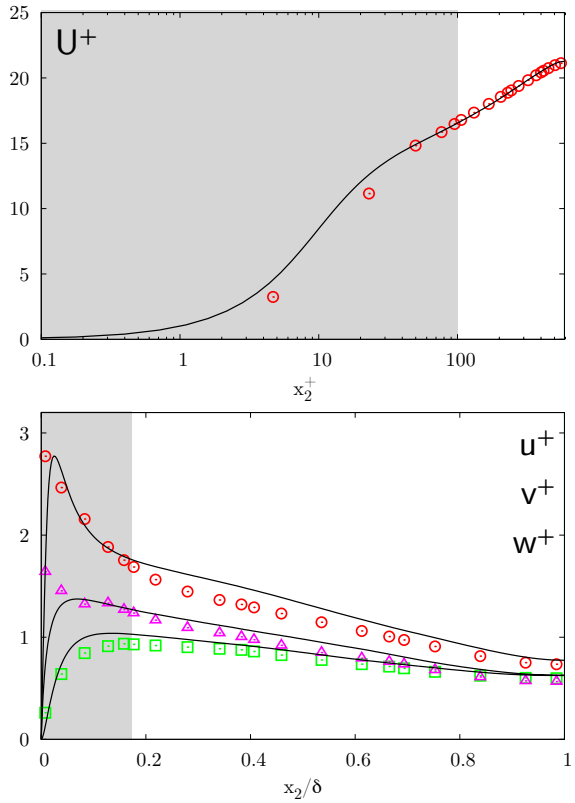

$Re_\tau = 2000$ (Δ^+: 98, 22–102, 98)

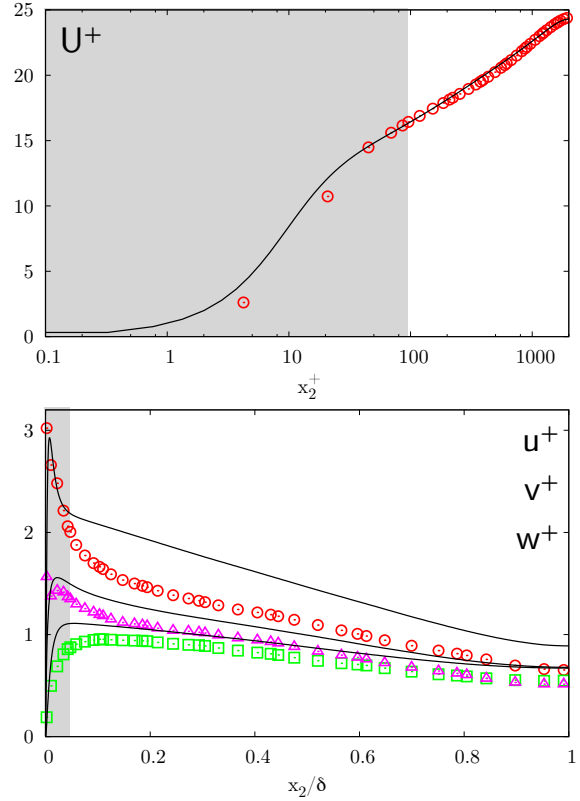

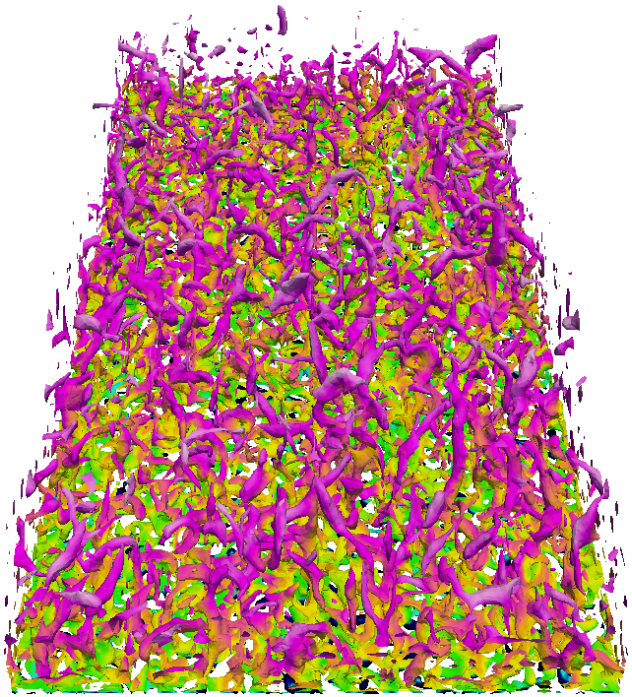

Iso-Q colored by velocity magnitude

LES with SD+WSM+LW

DNS Moser, et al., 1999 (Re_τ 590)
DNS Hoyas, Jiménez, 2006 (Re_τ 2000)

Modeled region

Moser, et al. (1999). Phys. Fluids, 11(4); Hoyas, Jiménez (2006). Phys. Fluids, 18; Breuer, Rodi (1996)

Wall-Modeled Turbulent Channel Flow

$\mathbf{Re_\tau = 590}$

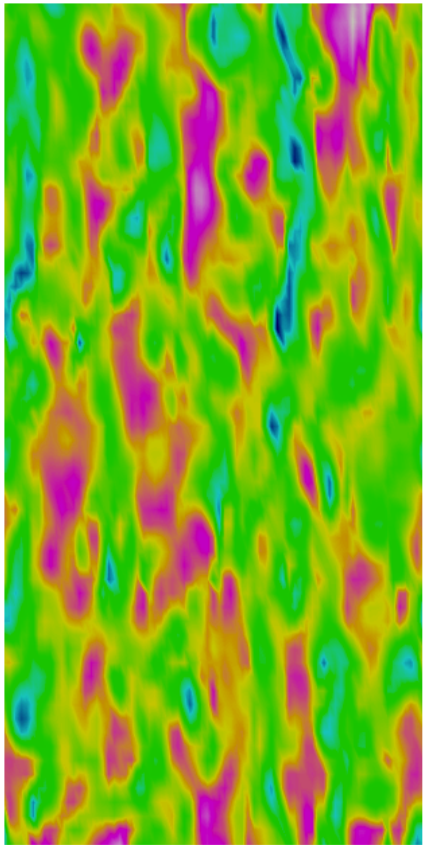

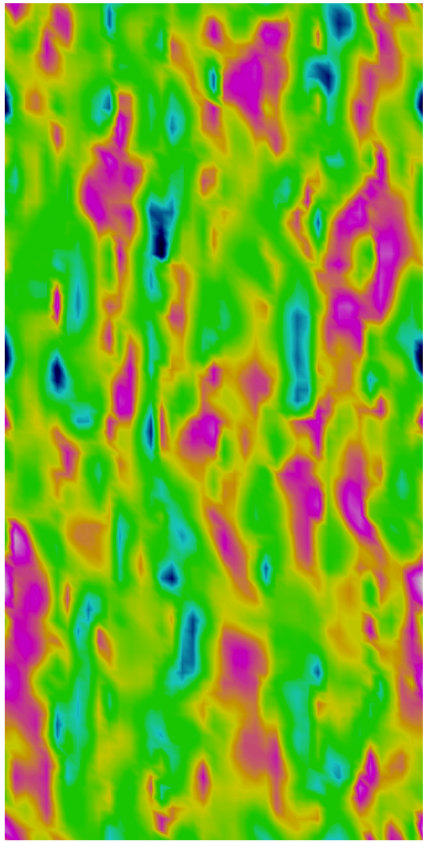

u at y^+=100

Wall-Resolved

Wall-Modeled

$\mathbf{Re_\tau = 2000}$

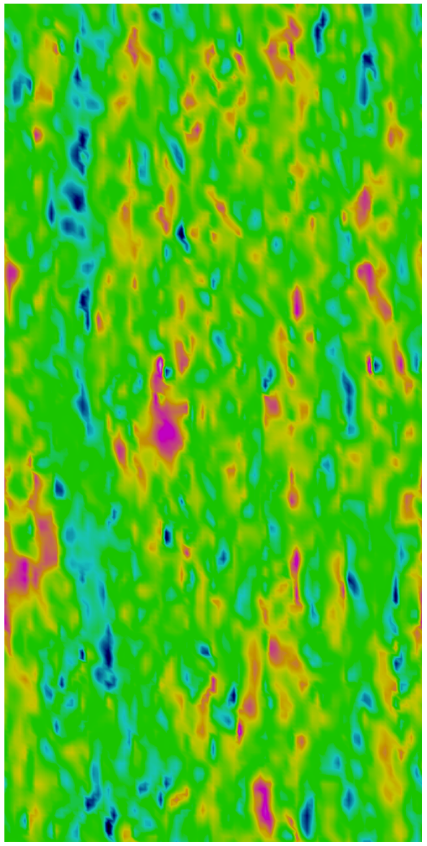

u at y^+=100

Flow Past Square Cylinder: Re = 21400

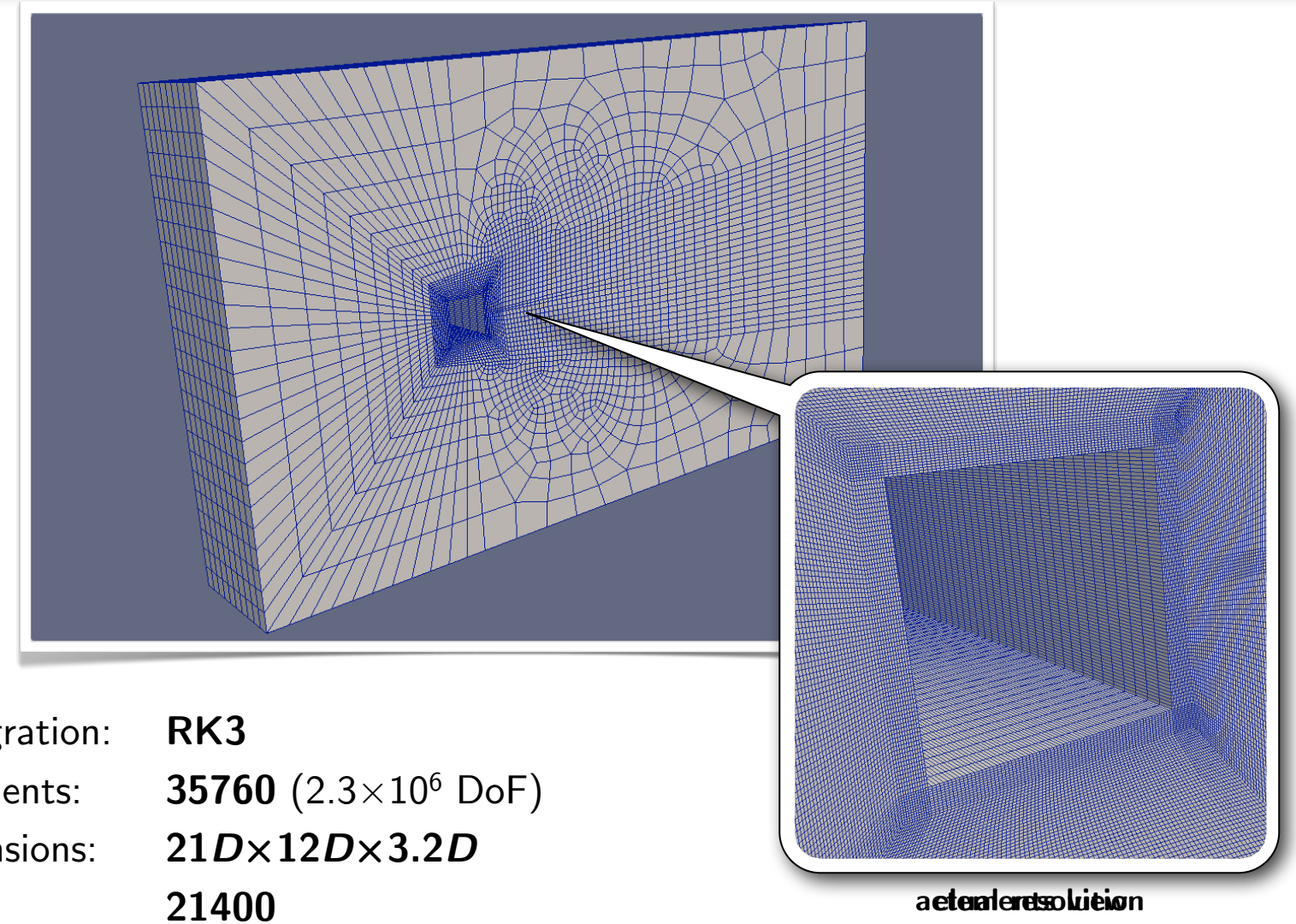

- Time integration: **RK3**
- Nº of elements: **35760** (2.3×10^6 DoF)
- Grid dimensions: $\mathbf{21}D\times\mathbf{12}D\times\mathbf{3.2}D$
- Reynolds: **21400**
- Mach: **0.3**
- Statistics: **16** T_0

Flow past a Square Cylinder: $Re_D = 21400$

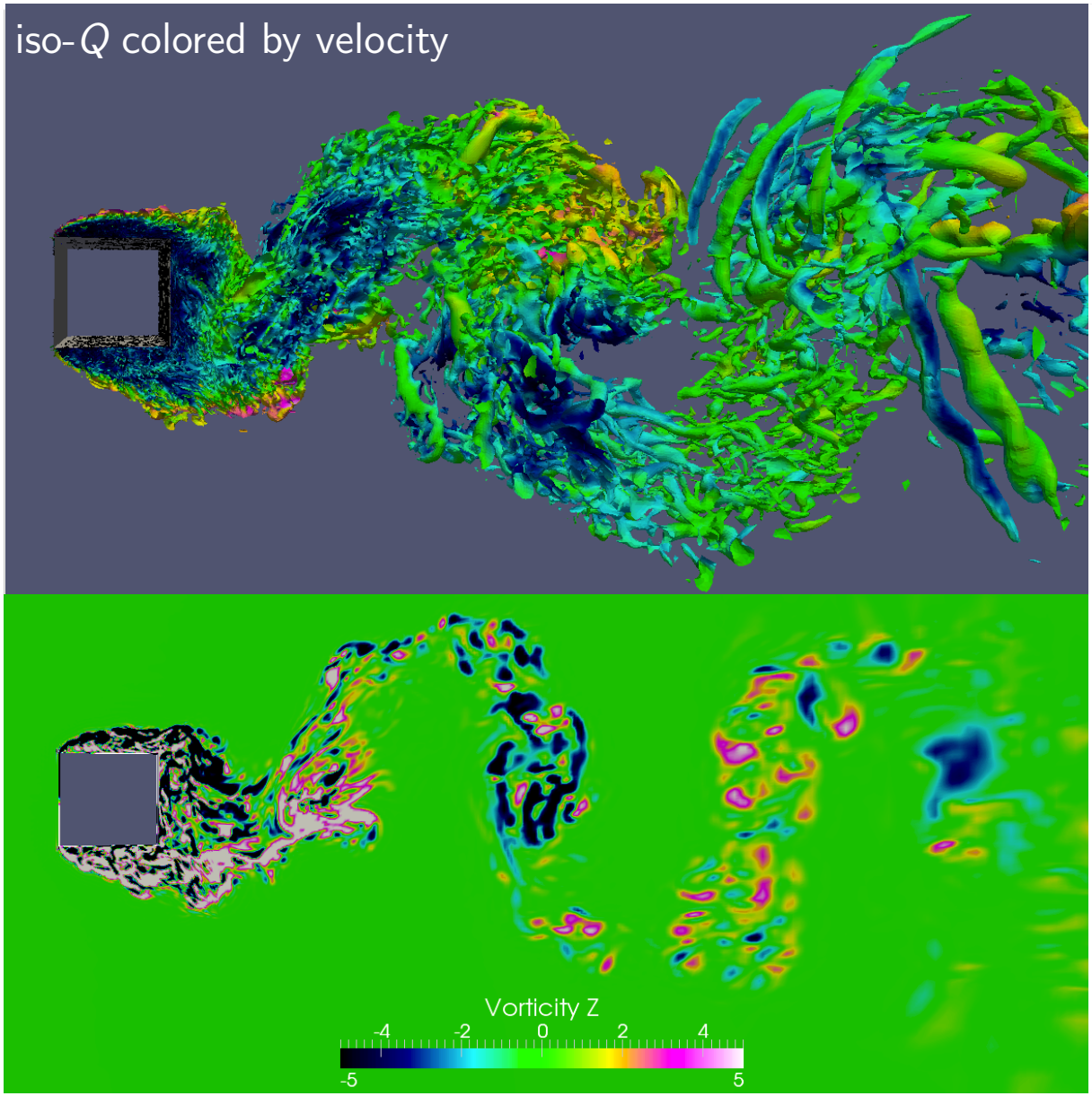

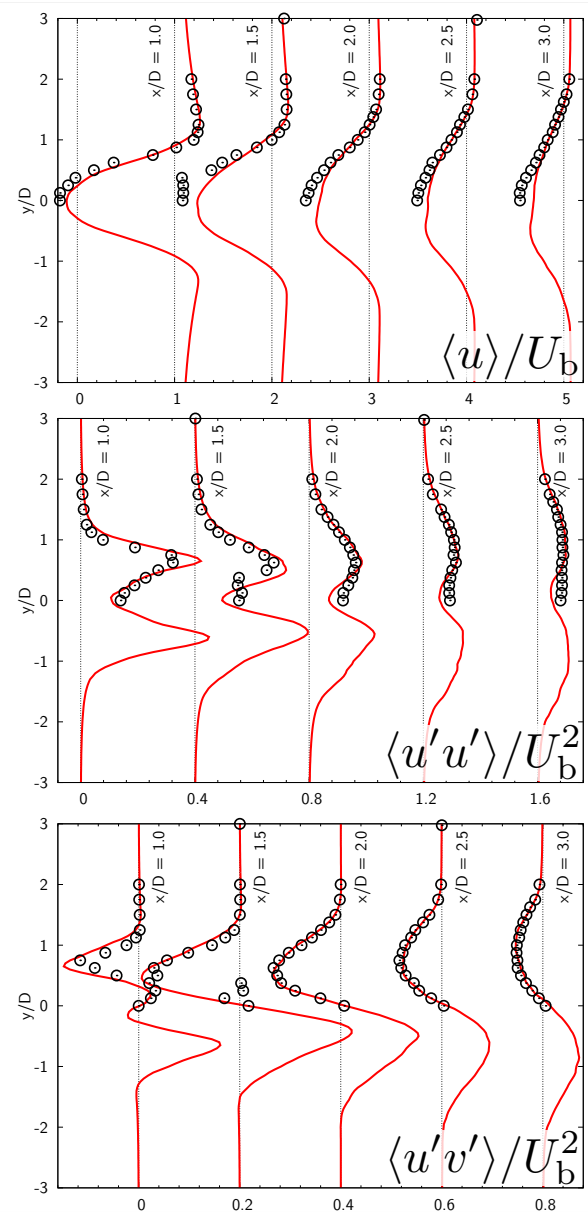

Preliminary results (work in progress)

Summary and Conclusions

Predicting the future is generally ill advised.
However, the following are the author's opinions:

- The early development of CFD in the Aerospace Industry was primarily driven by the need to calculate steady transonic flows: ***this problem is quite well solved***
- CFD has been on a plateau for the last 15 years with 2nd-order accurate FV methods for the RANS equations almost universally used in both commercial and government codes which can treat complex configurations
- These methods cannot reliably predict complex separated, unsteady and vortex dominated flows
- Ongoing advances in both numerical algorithms and computer hardware and software should enable an advance to LES for industrial applications within the foreseeable future
- Research should focus on high-order methods with minimal numerical dissipation for unstructured meshes to enable the treatment of complex configurations
- Eventually DNS may become feasible for high Reynolds number flows

hopefully with a smaller power requirement than a wind tunnel

Acknowledgement

The current research is a combined effort by

- *Postdocs*: Charlie Liang, Peter Vincent, Guido Lodato
- *Ph.D. students*: Sachin Premasuthan, Kui Ou, Patrice Castonguay, David Williams, Yves Allenau, Lala Li, Manuel López, and Andy Chan

It is made possible by the support of

- the *Airforce Office of Scientific Research* under grant FA9550-10-1-0418 by Dr. Fariba Fahroo
- the *National Science Foundation* under grants 0708071 and 0915006 monitored by Dr. Leland Jameson

A Review of the Literature from ACL

1. Castonguay, P., D. Williams, P. Vincent, M. Lopez, and A. Jameson (2011). On the development of a high-order, multi-GPU enabled, compressible viscous flow solver for mixed grids. *AIAA P.*, **vol. 2011-3229**
2. Jameson, A. (2010). A proof of the stability of the spectral difference method for all orders of accuracy. *J. Sci. Comput.*, **vol. 45**(1)
3. Jameson, A. (2011). Advances in bringing high-order methods to practical applications in computational fluid dynamics. *AIAA P.*, **vol. 2011-3226**
4. Jameson, A., P. Vincent, and P. Castonguay (2012). On the non-linear stability of flux reconstruction schemes. *J. Sci. Comput.*, **vol. 50**(2)
5. Lodato, G., P. Castonguay, and A. Jameson, Structural LES modeling with high-order spectral difference schemes. In *Annual Research Briefs* (Center for Turbulence Research, Stanford University, 2011)
6. Ou, K. and A. Jameson (2011). Unsteady adjoint method for the optimal control of advection and Burger's equations using high-order spectral difference method. *AIAA P.*, **vol. 2011- 24**
7. Vincent, P., P. Castonguay, and A. Jameson (2010). A new class of high-order energy stable flux reconstruction schemes. *J. Sci. Comput.*, **vol. 47**(1)
8. Vincent, P., P. Castonguay, and A. Jameson (2011). Insights from von Neumann analysis of high-order flux reconstruction schemes. *J. Comput. Phys.*, **vol. 230**(22)
9. Vincent, P. and A. Jameson (2011). Facilitating the adoption of unstructured high-order methods amongst a wider community of fluid dynamicists. *Math. Model. Nat. Phenom.*, **vol. 6**(3)
10. Williams, D., P. Castonguay, P. Vincent, and A. Jameson (2011). An extension of energy stable flux reconstruction to unsteady, non-linear, viscous problems on mixed grids. *AIAA P.*, **vol. 2011-3405**

ESFR Schemes for Quadrilateral Elements

ESFR Schemes for Quads

In the case of quadrilateral elements a natural approach is to use a tensor product to represent the discrete solution

$$u_h = \sum_{j=1}^{p+1} \sum_{n=1}^{p+1} u_{jn} l_j(x) n_n(y)$$

where $l_j(x)$ and $n_n(y)$ are Lagrange basis polynomials of degree p. In the case $p = 2$ this can be expanded as

$$u_h = a_1 + a_2 x + a_3 y + a_4 x^2 + a_5 xy + a_6 y^2 + a_7 x^2 y + a_8 xy^2 + a_9 x^2 y^2$$

Now

$$\nabla u_h = \begin{bmatrix} a_2 + 2a_4 x + a_5 y + 2a_7 xy + a_8 y^2 + 2a_9 xy^2 \\ a_3 + a_5 x + 2a_6 y + a_7 x^2 + 2a_8 xy + 2ax^2 y \end{bmatrix}$$

Now we assume that the divergence of the correction function can be represented by a polynomial with the same form as u_h:

$$\nabla \cdot \mathbf{g} = b_1 + b_2 x + b_3 y + b_4 x^2 + b_5 xy + b_6 y^2 + b_7 x^2 y + b_8 xy^2 + b_9 x^2 y^2$$

ESFR Schemes for Quads

Now, differentiating twice in both x and y, we find that

$$\frac{\partial}{\partial t} u_{h_{xxyy}} + \frac{\partial^2}{\partial x^2}\frac{\partial^2}{\partial y^2}\nabla \cdot \mathbf{g} = 0 \tag{4}$$

Now choose $\mathbf{g}$ such that

$$\int_D \mathbf{g} \cdot \nabla u_h dA = c\, u_{h_{xxyy}} \frac{\partial^2}{\partial x^2}\frac{\partial^2}{\partial y^2}\nabla \cdot \mathbf{g} = \int \frac{c}{4} u_{h_{xxyy}} \frac{\partial^2}{\partial x^2}\frac{\partial^2}{\partial y^2}\nabla \cdot \mathbf{g} dA$$

since both terms are constants. Thus using equation (4)

$$\int \mathbf{g} \cdot \nabla u_h dA = -\frac{c}{4}\int u_{h_{xxyy}} \frac{\partial}{\partial t} u_{h_{xxyy}} dA = -\frac{c}{4}\frac{d}{dt}\int u_{h_{xxyy}}^2 dA$$

and substituting for $\int \mathbf{g} \cdot \nabla u_h dA$ in equation (2) to get the following. Now on summing over the elements, a proper choice of the interface fluxes yields energy stability as before.

$$\frac{d}{dt}\int_D (\frac{u_h^2}{2} + \frac{c}{4} u_{h_{xxyy}}^2) dA + \int_B \mathbf{n} \cdot \mathbf{a} \frac{u_h^2}{2} dS + \int_B \mathbf{n} \cdot \mathbf{g} u_h dS = 0$$

ESFR Schemes for Quads

Hence

$$u_{h_{xxyy}} = 4a_9$$

$$\frac{\partial^2}{\partial x^2}\frac{\partial^2}{\partial y^2}\nabla \cdot \mathbf{g} = 4b_9$$

and

$$\begin{aligned}\int_D \mathbf{g} \cdot \nabla u_h dA \quad &= a_2 \int g_x dA + a_3 \int g_y dA \\ &\ldots \\ &+2a_9 \int (g_x xy^2 + g_y x^2 y) dA\end{aligned}$$

Hence to satisfy (4) all lower moments of $\mathbf{g}$ must vanish while

$$\int_D (g_x xy^2 + g_y x^2 y) dA = 8cb_9$$

ESFR Schemes for Quads

Now we can integrate by parts to obtain conditions directly for the moments of $\nabla \cdot \mathbf{g}$

$$\int_D \nabla \cdot \mathbf{g} dV = \int \mathbf{g} \cdot \mathbf{n} dS + 0$$

$$\int_D \nabla \cdot \mathbf{g} x dV = \int \mathbf{g} \cdot \mathbf{n} x dS + 0$$

$$\int_D \nabla \cdot \mathbf{g} y dV = \int \mathbf{g} \cdot \mathbf{n} y dS + 0$$

$$\ldots$$

$$\int_D \nabla \cdot \mathbf{g} x^2 y^2 dV = \int \mathbf{g} \cdot \mathbf{n} x^2 y^2 dS + 16 c b_9$$

These moment conditions are sufficient to define $\nabla \cdot \mathbf{g}$ uniquely. The nodal DG scheme is recovered by setting $c = 0$. In this case the equations for the coefficients of $\nabla \cdot \mathbf{g}$ can be solved with $\nabla \cdot \mathbf{g}$ expressed in the form of a tensor product. However, if $c \neq 0$ the solution for $\nabla \cdot \mathbf{g}$ can no longer be expressed as a tensor product.

ESFR Schemes for 3D Pyramids

ESFR Schemes for Pyramids

For pyramids, using polynomials of degree 2, we can represent u_h and $\nabla \cdot \mathbf{g}$ as

$$\begin{aligned} u_h =& a_1 + a_2 x + a_3 y + a_4 x^2 + a_5 xy + a_6 y^2 + a_7 x^2 y + a_8 xy^2 + a_9 x^2 y^2 + \\ & a_{10} z + a_{11} xz + a_{12} yz + a_{13} z^2 + a_{14} xyz \end{aligned}$$

and

$$\begin{aligned} \nabla \cdot \mathbf{g} =& b_1 + b_2 x + b_3 y + b_4 x^2 + b_5 xy + b_6 y^2 + b_7 x^2 y + b_8 xy^2 + b_9 x^2 y^2 + \\ & b_{10} z + b_{11} xz + b_{12} yz + b_{13} z^2 + b_{14} xyz \end{aligned}$$

The energy stability for 3D pyramids requires all moments of $\mathbf{g}$ to vanish except

$$\int_D (g_x xy^2 + g_y x^2 y) dV = 8 c_1 b_9$$

$$\int_D (g_z z) dV = 2 c_2 b_{13}$$

$$\int_D (g_x yz + g_y xz + g_z xy) dV = c_3 b_{14}$$

ESFR Schemes for Pyramids

Then

$$\frac{\partial}{\partial t}\mathbf{u_h}_{xxyy} + \frac{\partial^2}{\partial x^2}\frac{\partial^2}{\partial y^2}\nabla\cdot\mathbf{g} = 0$$

$$\frac{\partial}{\partial t}\mathbf{u_h}_{zz} + \frac{\partial^2}{\partial z^2}\nabla\cdot\mathbf{g} = 0$$

$$\frac{\partial}{\partial t}\mathbf{u_h}_{xyz} + \frac{\partial}{\partial x}\frac{\partial}{\partial y}\frac{\partial}{\partial z}\nabla\cdot\mathbf{g} = 0$$

The requirement to ensure energy stability becomes

$$\int_D \mathbf{g}\cdot\nabla u_h dA = \frac{1}{2}\frac{d}{dt}\int_D \left(c_1\ u_{h\,xxyy}^2 + c_2\ u_{h\,zz}^2 + c_3\ u_{h\,xyz}^2\right) dV$$

ESFR Schemes for Pyramids

After integration by parts $\nabla \cdot \mathbf{g}$ can be determined from 14 moments

$$\int_D \nabla \cdot \mathbf{g} dV = \int \mathbf{g} \cdot \mathbf{n} dS + 0$$

$$\int_D \nabla \cdot \mathbf{g} x dV = \int \mathbf{g} \cdot \mathbf{n} x dS + 0$$

$$\int_D \nabla \cdot \mathbf{g} y dV = \int \mathbf{g} \cdot \mathbf{n} y dS + 0$$

$$\int_D \nabla \cdot \mathbf{g} z dV = \int \mathbf{g} \cdot \mathbf{n} z dS + 0$$

$$\ldots$$

$$\int_D \nabla \cdot \mathbf{g} x^2 y^2 dV = \int \mathbf{g} \cdot \mathbf{n} x^2 y^2 dS + 16 c_1 b_9$$

$$\int_D \nabla \cdot \mathbf{g} z^2 dV = \int \mathbf{g} \cdot \mathbf{n} z^2 dS + 4 c_2 b_{13}$$

$$\int_D \nabla \cdot \mathbf{g} xyz dV = \int \mathbf{g} \cdot \mathbf{n} xyz dS + c_3 b_{14}$$

Energy Stable Implicit Crank-Nicolson Type Scheme

Energy Stable Implicit Crank-Nicolson

In order to preserve true energy stability with the time integration scheme one ought to use an implicit scheme of Crank-Nicolson type. Using a superscript n to denote the time level, let

$$\bar{u}_h = \frac{1}{2}(u_h^{n+1} + u_h^n)$$

Suppose now that all terms in the space discretization are evaluated using $\bar{u}_h$. Then the scheme is

$$u_h^{n+1} = u_h^n - \Delta t(a\frac{\partial \bar{u}_h}{\partial x} + f_{cl}g_l' + f_{cr}g_r')$$

where f_{cl} and f_{cr} are calculated from $\bar{u}_h$ in the adjacent cells. Moreover, differentiating p times

$$u_h^{(p)^{n+1}} - u_h^{(p)^n} = -\Delta t(f_{cl}g_l^{p+1} + f_{cr}g_r^{p+1})$$

Energy Stable Implicit Crank-Nicolson

Now, multiplying by $\bar{u}_h$ and integrating over the element

$$\frac{1}{2}\int_{-1}^{1} u_h^{n+1^2}dx - \frac{1}{2}\int_{-1}^{1} u_h^{n^2}dx = -\Delta t\left[a\int_{-1}^{1}\bar{u}_h\frac{\partial \bar{u}_h}{\partial x}dx + f_{cl}\int_{-1}^{1}\bar{u}_h g_l' dx + f_{cr}\int_{-1}^{1}\bar{u}_h g_r' dx\right]$$
$$= -\Delta t\left[\frac{a}{2}(\bar{u}_h(1)^2 - \bar{u}_h(-1^2)) + f_{cr}\bar{u}_h(1) - f_{cl}\bar{u}_h(-1)\right]$$
$$+\Delta t\left[f_{cr}\int_{-1}^{1} g_r\frac{\partial \bar{u}_h}{\partial x}dx + f_{cl}\int_{-1}^{1} g_l\frac{\partial \bar{u}_h}{\partial x}dx\right]$$

Choosing g_r and g_l as in section II such that

$$\int g_r\frac{\partial \bar{u}_h}{\partial x} = cg_r^{(p+1)}\bar{u}_h^{(p)}, \int g_l\frac{\partial \bar{u}_h}{\partial x} = cg_l^{(p+1)}\bar{u}_h^{(p)}$$

The last term is equivalent to

$$-\frac{c}{2}(u_h^{(p)^{n+1}} - u_h^{(p)^n})(u_h^{(p)^{n+1}} + u_h^{(p)^n}) = -\frac{c}{2}(u_h^{(p)^{n+1^2}} - u_h^{(p)^{n^2}})$$

Energy Stable Implicit Crank-Nicolson

Accordingly on summing over the elements with a proper choice of the interface flux, and transforming the reference element to the physical elements, the broken norm

$$\sum_{elements} \int_{x_n}^{x_{n+1}} \left(\frac{u_h^2}{2} + \frac{c}{4} h_n^{2p} {u_h^{(p)}}^2\right)^2 dx$$

is strictly non-increasing.